Crustal structure of the northern Nova Scotia rifted continental margin (eastern Canada)

Thomas Funck,[1] H. Ruth Jackson,[2] Keith E. Louden,[3] Sonya A. Dehler,[2] and Yue Wu[4]

Received 5 February 2004; revised 24 June 2004; accepted 12 July 2004; published 21 September 2004.

[1] The Nova Scotia continental margin off eastern Canada marks a transition from a volcanic to a nonvolcanic style of rifting. The northern (nonvolcanic) segment of the margin was studied by a 490-km-long refraction seismic line with dense air gun shots, coincident with previous deep reflection profiles. A *P* wave velocity model was developed from forward and inverse modeling of the wide-angle data from 19 ocean bottom seismometers and coincident normal incidence reflection profiles. The continental crust has a maximum thickness of 36 km and is divided into three layers with velocities of 5.7–6.9 km/s. Crustal thinning down to 3 km occurs in a 180-km-wide zone and the sediment cover in this area is up to 15 km thick. Farther seaward, a 150-km-wide transition zone is observed with a 5-km-thick lower layer (7.2–7.6 km/s) interpreted as partially serpentinized mantle. At the landward end, this layer is overlain by highly altered continental crust (5.4 km/s) extending up to the seaward limit of the Jurassic salt province. Farther seaward, the upper layer is interpreted as exhumed and highly serpentinized mantle (5.1 km/s) separated from the lower layer by subhorizontal reflectivity, which probably represents a serpentinization front. Oceanic crustal thickness is 4 km with layer 2 velocities of 4.6–5.0 km/s. Layer 3 velocities of 6.4–6.55 km/s are lower than typical lower oceanic crust velocities but consistent with a low magma supply and increased tectonism as observed on the reflection profile. This reduced magma production might be related to the proximity of the Newfoundland transform margin. *INDEX TERMS:* 8105 Tectonophysics: Continental margins and sedimentary basins (1212); 3025 Marine Geology and Geophysics: Marine seismics (0935); 7205 Seismology: Continental crust (1242); 7220 Seismology: Oceanic crust; 9325 Information Related to Geographic Region: Atlantic Ocean; *KEYWORDS:* continental margins, mantle serpentinization, crustal structure

Citation: Funck, T., H. R. Jackson, K. E. Louden, S. A. Dehler, and Y. Wu (2004), Crustal structure of the northern Nova Scotia rifted continental margin (eastern Canada), *J. Geophys. Res.*, *109*, B09102, doi:10.1029/2004JB003008.

1. Introduction

[2] The continental margin off Nova Scotia, Canada, marks the transition from volcanic style margins to the south (U.S. East Coast) [e.g., *Holbrook and Kelemen*, 1993; *Holbrook et al.*, 1994b] to nonvolcanic style margins to the north (Newfoundland and Labrador) [e.g., *Reid*, 1994; *Chian et al.*, 1995a; *Louden and Chian*, 1999; *Funck et al.*, 2003]. Off Nova Scotia, the East Coast Magnetic Anomaly (ECMA) progressively weakens northward and eventually disappears (Figure 1). *Keen and Potter* [1995a] noted a correlation between seaward dipping reflections (SDR) and the ECMA where they are well developed on the southern part of the margin. Deep marine reflection seismic profiles show SDR units on lines 89-3 and 89-4 [*Keen and Potter*, 1995a] across the high-amplitude ECMA (~300 nT) on the western segment of the Nova Scotia margin (Figure 1). Along line 88-1A [*Keen et al.*, 1991] on the middle segment of the margin, the amplitude of the ECMA has decreased to ~180 nT, and there is no evidence of SDR. The eastern margin segment, where the ECMA has disappeared (line 89-1), has been classified as a nonvolcanic rifted margin [*Keen and Potter*, 1995b].

[3] Despite numerous deep reflection seismic lines along the Nova Scotia margin, there is an absence of modern refraction seismic data, which would allow the velocity structure of along-strike variations of the margin to be investigated. Previous refraction seismic data (see summary of *Keen et al.* [1990b] and *Keen and Cordsen* [1981]) are limited to the shelf and slope but do not extend into the deeper basin. The Scotian Margin Transects (SMART) refraction seismic experiment (Figure 1) was designed to image the along-strike variation in crustal structure over the transition from a volcanic to a nonvolcanic style of rifting. This is critical for understanding why the margin appears nonvolcanic to the northeast. *Keen and Potter* [1995b]

[1]Danish Lithosphere Centre, Copenhagen, Denmark.
[2]Geological Survey of Canada (Atlantic), Bedford Institute of Oceanography, Dartmouth, Nova Scotia, Canada.
[3]Department of Oceanography, Dalhousie University, Halifax, Nova Scotia, Canada.
[4]Department of Earth Sciences, Dalhousie University, Halifax, Nova Scotia, Canada.

Copyright 2004 by the American Geophysical Union.
0148-0227/04/2004JB003008$09.00

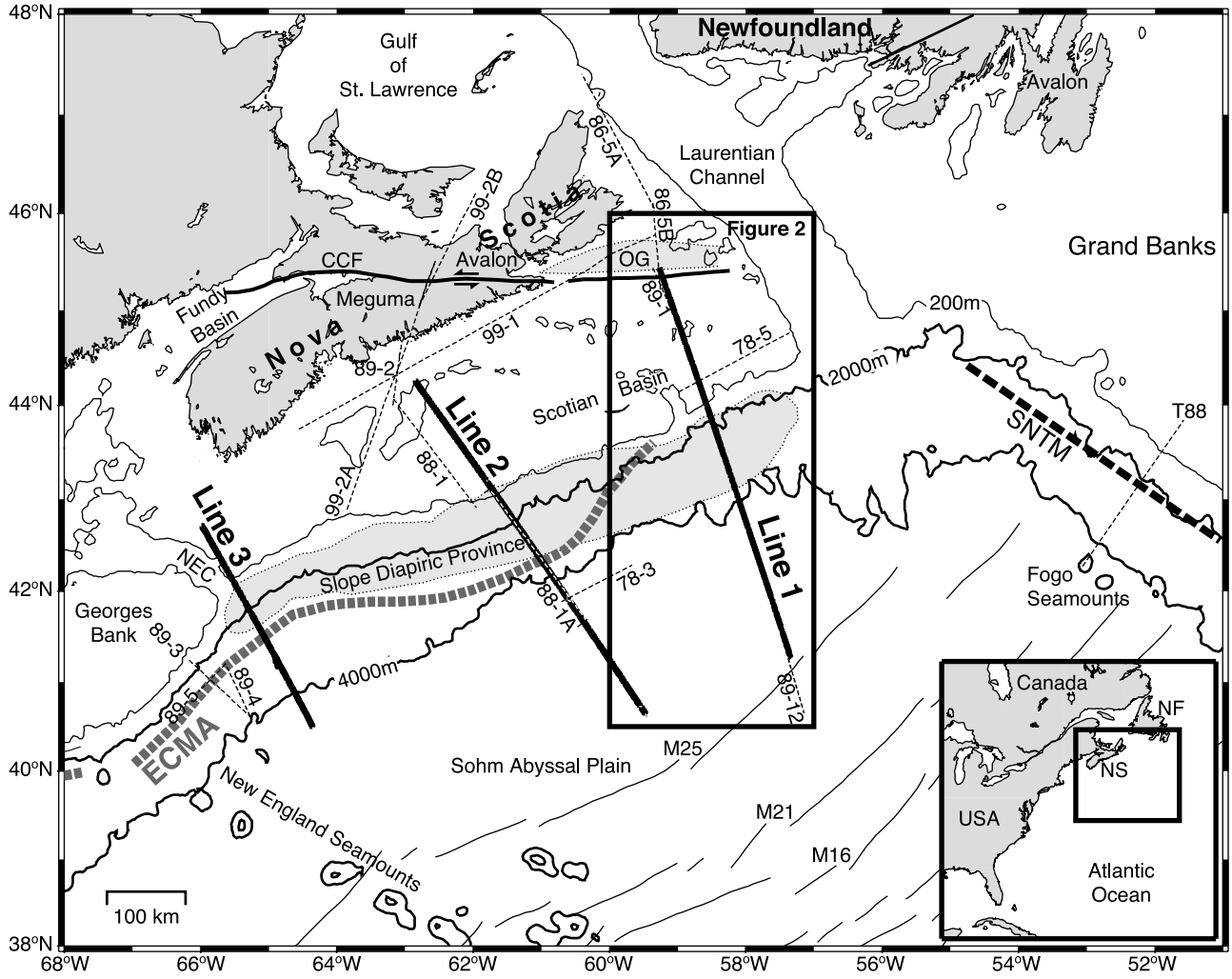

Figure 1. Location map of the Nova Scotia margin. The 200-m bathymetric contour is shown as thin solid line, the 2000-m and 4000-m contours are indicated by solid lines. The center of the East Coast Magnetic Anomaly (ECMA) is marked by a dashed gray line, and the southeast Newfoundland transform margin (SNTM) is marked by a bold dashed line. Shaded areas outlined by dotted lines indicate the location of the Jurassic salt of the Slope Diapiric Province and of the Paleozoic Orpheus Graben (OG). Magnetic anomalies are shown as solid lines. The three refraction seismic lines of the SMART experiment are marked by bold solid lines. Other relevant seismic lines in the study area are shown as dashed lines: line 89-12 (unpublished data by the German Federal Agency of Natural Resources and Geosciences, BGR); lines 78-3 and 78-5 [*Keen and Cordsen*, 1981]; line T88 [*Todd et al.*, 1988]; line 89-1 [*Keen and Potter*, 1995b]; lines 88-1 and 88-1A [*Keen et al.*, 1991]; lines 86-5A and 86-5B [*Marillier et al.*, 1989]; lines 89-3, 89-4, and 89-5 [*Keen and Potter*, 1995a]; and lines 99-1, 99-2A, and 99-2B [*Salisbury and Jackson*, 2003]. Faults are shown as bold solid lines, and arrows indicate the sense of displacement. Abbreviations are NS, Nova Scotia; NF, Newfoundland, CCF, Cobequid Chedabucto fault; NEC, Northeast Channel.

suggested a model in which the change in volcanism is related to differences in prerift lithospheric properties that control the geometry and width of the rift. As the width of the rift zone decreases southward, the narrower zone of necking might create an opportunity for more vigorous rift-related small-scale convection in the asthenosphere, which could enhance the production of igneous rocks.

[4] Studies on mantle decompression during rifting show that melt generation is strongly dependent on rift duration. If the rifting lasts long enough, little or no melt is produced [*Bown and White*, 1995] due to conductive cooling of the upwelling asthenosphere. In contrast, other modeling results suggest that an increase in extension rate will result in a decrease of the length of synextensional magmatic episodes [*Harry and Bowling*, 1999], while 5–7 km of new oceanic crust can be generated at the time of breakup.

[5] In this paper, the results from the easternmost refraction seismic line of the SMART experiment are presented (line 1, Figures 1 and 2). This line lies within the nonvolcanic margin segment and is coincident with the deep reflection seismic line 89-1 of *Keen and Potter* [1995b]. The reflection line shows significant thinning of the conti-

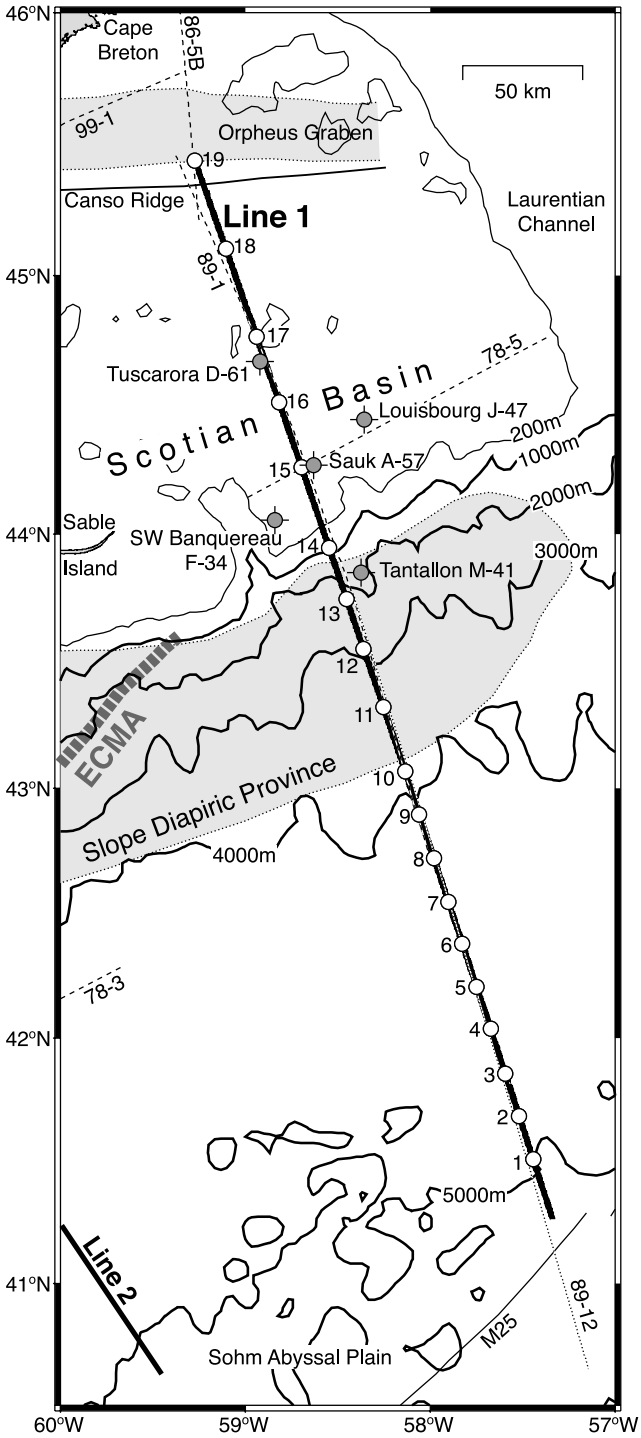

Figure 2. Location map for SMART line 1 (bold solid line). Positions of ocean bottom seismometers are indicated by open circles with the instrument number given. Solid circles on top of crosses mark the location of deep exploration wells in the vicinity of line 1. MCS line BGR 89-12 is shown as dotted line. Other features are as described in Figure 1.

nental crust over a 200-km-wide zone. Seaward of this is a 200-km-wide transitional region with thin (<9 km) crust of unknown character. Velocity information from refraction line 1 will provide more information to determine the nature of this crust. In addition, seaward extension of the refraction seismic profile along another coincident multichannel seismic (MCS) profile (BGR line 89-1) will help to resolve the nature of the transition into oceanic crust.

2. Geological Setting

[6] The Nova Scotia margin (Figure 1) is part of the North American–northwest African conjugate margin pair that formed during the Mesozoic breakup of Pangea [*Klitgord and Schouten*, 1986]. The margin was formed within rocks of the Appalachian orogen. Onshore, southern Nova Scotia lies within the Meguma terrane, while the northeast is part of the Avalon terrane [*Barr and Raeside*, 1989], which continues to eastern Newfoundland and the Grand Banks [*Williams*, 1979, 1995]. Triassic basins like the Fundy and Orpheus Basins resulted from strike-slip convergent tectonics along the Cobequid-Chedabucto fault system at the Avalon-Meguma terrane boundary [*Gibling et al.*, 1987]. Rifting of the Nova Scotia margin was characterized by Late Triassic–Early Jurassic continental extension (rift phase), followed by Jurassic-Tertiary ocean opening and passive margin development (drift phase) [*Welsink et al.*, 1989]. The rifting terminated at around 175 Ma with the separation from Africa [*Klitgord and Schouten*, 1986].

[7] The Scotian Basin along the northeastern Nova Scotia margin is up to 18 km deep. Oldest dated deposits in the basin are of Late Triassic age [*Wade and MacLean*, 1990]. Numerous salt diapirs (Argo salt) of probably Late Triassic–Early Jurassic age can be found in the Slope Diapiric Province (Figure 1) [*Welsink et al.*, 1989]. The continent-ocean boundary is thought to lie seaward of the salt front [*Keen and Potter*, 1995b]. The stratigraphy of the Sohm Abyssal Plain at the seaward limit of the study area is summarized by *Ebinger and Tucholke* [1988].

3. Wide-Angle Seismic Experiment

3.1. Data Acquisition and Processing

[8] The SMART wide-angle reflection/refraction seismic experiment was carried out in 2001 onboard the Canadian Coast Guard ship *Hudson*. The easternmost transect (line 1) is 490 km long and runs from the Orpheus Graben in the north, across the Scotian Basin and the Slope Diapiric Province into the Sohm Abyssal Plain (Figure 2). The northernmost 315 km of line 1 are coincident with deep reflection seismic line 89-1, acquired by the Geological Survey of Canada [*Keen and Potter*, 1995b]; while its southernmost 292 km are parallel to an unpublished reflection seismic profile (line 89-12) of the German Federal Agency of Geosciences and Natural Resources (BGR).

[9] Nineteen ocean bottom seismometers (OBS) of the Geological Survey of Canada and Dalhousie University were deployed along line 1. These instruments are equipped with a hydrophone and three-component 4.5-Hz geophones. Instrument spacing varied from 40 km on the shelf to 20 km in the deep basin. The seismic source was a tuned air gun array with a total volume of 104 L, consisting of 12 individual guns ranging in volume from 2.6 to 16.4 L. The array was fired once per minute at an average ship's speed of 4.3 knots, resulting in an average shot spacing of 132 m.

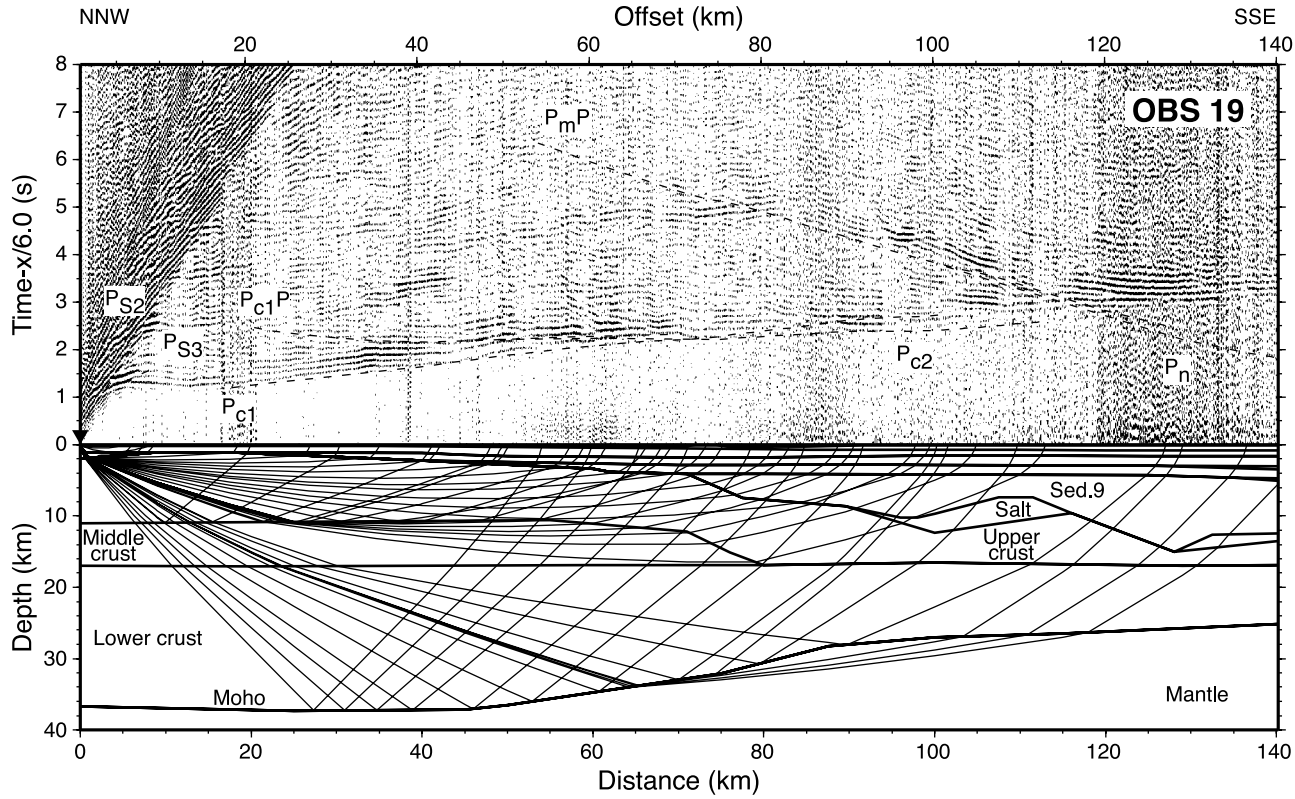

Figure 3. (top) Record section with computed travel times and (bottom) ray path diagram for the vertical geophone of OBS 19. Horizontal scale in the record section is shot-receiver distance (offset), and the vertical scale is the travel time using a reduction velocity of 6.0 km/s. Triangle indicates the receiver location. See text for description of phases and processing. The horizontal scale of the ray path diagram is distance along the velocity model (Figure 9). Sed. 9 is sediment layer 9.

[10] For navigation (OBS and shot locations) and shot timing, the Global Positioning System (GPS) was used. Water depths along the transect were obtained by converting measurements from the ship's echo sounder using a depth-velocity function derived from a conductivity-temperature-depth (CTD) measurement at the southeastern end of line 2 to a depth of 2109 m, with downward extrapolation for greater depths.

[11] OBS data were converted to SEGY format, and time corrections for the drift of the OBS clock were applied. Data were debiased and resampled to 10 ms. Travel time picks of the direct wave were used to recalculate the position of the instrument at the seafloor, from which the shot-receiver ranges were calculated. The seismic data were deconvolved to sharpen the wavelet, and a band-pass filter from 4 to 10 Hz was applied. Traces in the record sections in Figures 3–6 are weighted by their distance to the OBS to increase amplitudes for large offsets.

3.2. Methodology

[12] The baseline for the two-dimensional velocity modeling was defined by a great circle arc through OBS 19 (corresponding to a horizontal distance of x = 0 km in the model) and the southeasternmost shot (corresponding to x = 489.86 km). After recalculation of the OBS locations using the direct wave, instrument positions were projected onto this baseline.

[13] The velocity model for the crust and uppermost mantle was developed using the program RAYINVR [*Zelt and Smith*, 1992; *Zelt and Forsyth*, 1994]. First, observed travel times were fitted by forward modeling, with the model developed from top to bottom. Down to the basement, the layer geometry in the velocity model is mostly derived from correlation with the coincident MCS data. The choice of sediment layers is based on changes in the slope of the refraction travel time curve, which are generally also distinguishable in the seismic reflection data. However, on the shelf down to a depth of ~4 km, refraction layer boundaries are more or less horizontal, while reflection data indicate a gentle SE dip of the layer strata. Salt lenses introduced to the model are strictly based on their identification on MCS line 89-1 [*Keen and Potter*, 1995b] since they could not be resolved by the refraction data. A velocity of 4.45 km/s was used for the salt, which is the mean value determined from drilling results [*Shimeld*, 2004]. Below basement, the normal incidence reflectivity becomes less continuous although some Moho and intracrustal reflectivity can be identified and correlated with the wide-angle data. In a second step, velocities within individual layers were recalculated by using the inversion algorithm in RAYINVR. Upon changes in the velocity model, layer boundaries were adjusted to keep the match with the two-way travel times in the MCS data.

3.3. Seismic Data

[14] All OBS were successfully recovered after the experiment although technical problems prevented the recording of data on OBS 4. However, this OBS was not

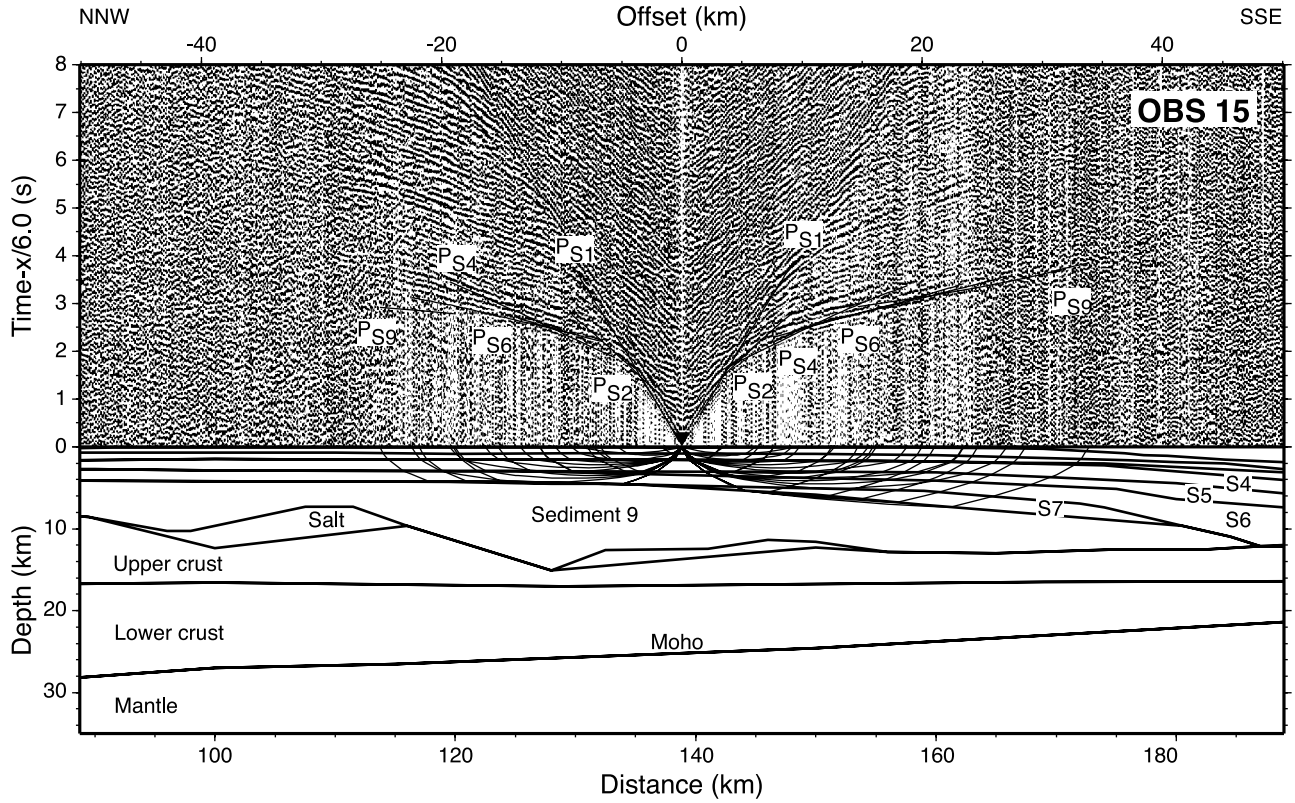

Figure 4. (top) Record section with computed travel times and (bottom) ray path diagram for the vertical geophone of OBS 15. Horizontal scale in the record section is shot-receiver distance (offset), and the vertical scale is the travel time using a reduction velocity of 6.0 km/s. Triangle indicates the receiver location. See text for description of phases and processing. The horizontal scale of the ray path diagram is distance along the velocity model (Figure 9). S4 to S9 indicate sediment layers.

at a critical location since both neighboring instruments show the same velocity structure. Data quality is generally good even though there are some stations with a lower signal-to-noise ratio, which can be attributed to complications associated with the deep Scotian Basin, as discussed below. Refractions were recorded for offsets up to 150 km.

[15] The phase nomenclature used in this paper is based on the later interpretation of individual layers in the velocity model. Refractions within the nine sedimentary layers are labeled P_{S1} through P_{S9}, while the reflections from the base of each of these layers are named $P_{S1}P$ through $P_{S9}P$. P_BP is the basement reflection. P_{c1} through P_{c3} are refractions within the continental crust, $P_{c1}P$ and $P_{c2}P$ are midcrustal reflections. Refractions within oceanic layers 2 and 3 are named P_{L2} and P_{L3}, respectively. P_mP is the Moho reflection. Two layers in the transition zone, which are later interpreted as serpentinized mantle, are characterized by refractions labeled P_{n1} and P_{n2}, and by reflections from their base ($P_{m1}P$ and $P_{m2}P$). Refractions within "normal" (i.e., unserpentinized) mantle are named P_n.

[16] Some key record sections are presented in Figures 3–6, which show the suite of crustal structures encountered along the profile. The landwardmost station OBS 19 (Figure 3) characterizes the full thickness continental crust. Phase velocities of the upper and middle crustal refractions (P_{c1} and P_{c2}) are 5.3 and 5.6 km/s, respectively. These phase velocities are rather low for rocks found elsewhere within the Appalachian orogen [see *Hall et al.*, 1998] but are related to the seaward thickening of the sediments in the Scotian Basin, resulting in a phase velocity smaller than the rock velocity. A reflection ($P_{c1}P$) delineates the boundary between the upper and middle crust. This phase can be correlated for offsets >20 km. The P_mP phase becomes a clearly recognizable phase for offsets >85 km, although some weak energy of precritical P_mP arrivals can be traced back to an offset of 55 km.

[17] Record sections within the deep Scotian Basin are characterized by reduced signal-to-noise ratios for larger offsets when compared to other OBS. An example of this is OBS 15 (Figure 4), where a series of refractions within the sedimentary column (P_{S1} through P_{S9}) can be correlated for offsets of up to ~30 km. For larger offsets, hardly any coherent seismic energy is discernable. The reason for this lies within the lower sediment layer (sediment 9), which is not as homogenous as it appears in the velocity model. The 6-km-deep exploration well Louisbourg J-47 (BASIN database, Geological Survey of Canada, Dartmouth, Nova Scotia, Canada) some 30 km off line 1 (Figure 2) shows that the top of sediment layer 9 is composed of interbedded carbonate (limestone) and sand with logging velocities in the range from 3.5 to 6.0 km/s with a clear low-velocity zone. Additional low-velocity zones are possible in the underlying 8 km of sediments that were not drilled, especially as salt is interpreted on reflection line 89-1 close to basement [*Keen and Potter*, 1995b]. Hence the problems with the lack of seismic energy for larger offsets are

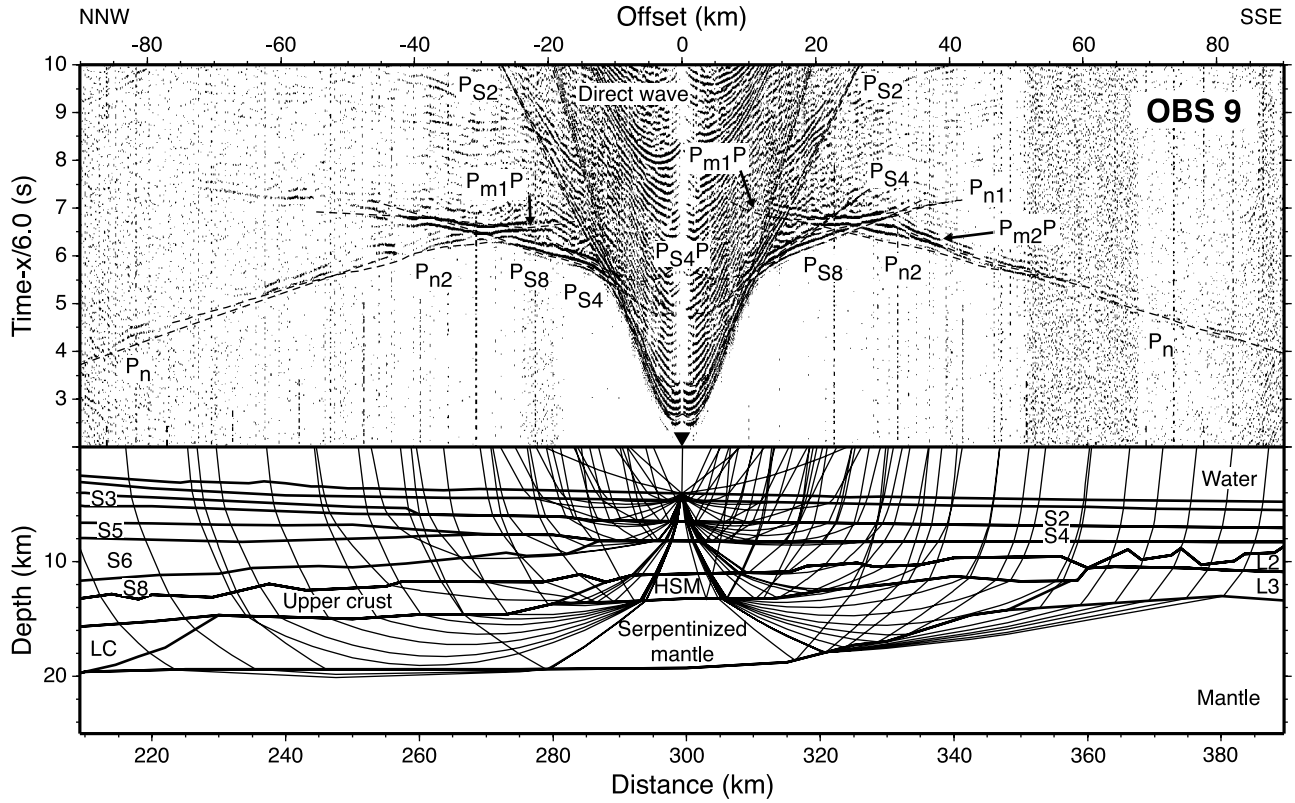

Figure 5. (top) Record section with computed travel times and (bottom) ray path diagram for the vertical geophone of OBS 9. Horizontal scale in the record section is shot-receiver distance (offset), and the vertical scale is the travel time using a reduction velocity of 6.0 km/s. Triangle indicates the receiver location. See text for description of phases and processing. The horizontal scale of the ray path diagram is distance along the velocity model (Figure 9). Abbreviations are S2 to S8, sediment layers; LC, lower crust; HSM, highly serpentinized mantle; L2 and L3, oceanic crustal layers 2 and 3.

attributed to a complex velocity structure within the lower sedimentary unit.

[18] OBS 9 (Figure 5) is located in the transition zone between continental and oceanic crust. The record section shows refractions (P_{n1} and P_{n2}) from two layers. The velocity contrast of ~2 km/s between these two layers creates a strong reflection ($P_{m1}P$) on either side of the instrument. However, a wide-angle reflection from the base of the lower layer ($P_{m2}P$) is only observed to the southeast of the instrument, starting at an offset of 32 km. To the southeast there is also a clear decrease in amplitude from stronger refractions in the lower layer (P_{n2}) to weaker ones in the normal mantle (P_n), occurring at an offset of ~60 km. This indicates a higher-velocity gradient in the lower layer than in the normal mantle.

[19] OBS 6 (Figure 6) is probably the key record section of line 1 since it is located right at the boundary between the transition zone in the northwest and oceanic crust in the southeast. This is imaged by differences in the observed phases on either side of the instrument. To the northwest, there is a high-amplitude P_{n2} phase with a phase velocity of 7.0 km/s, which is not observed to the southeast. Instead there are two refractions P_{L2} and P_{L3} with phase velocities of 4.7 and 6.0 km/s, respectively. The P_{L2} phase is best seen between offsets of 17 and 22 km where it shows up as a branch between the P_{L3} phase and the refraction from the lowermost sediment layer (P_{S8}). Figures 7 and 8summarize the observed and calculated travel times for all stations.

4. Results

4.1. Velocity Model

[20] The *P* wave velocity model for SMART line 1 is shown in Figure 9. Sediments are divided in nine layers (S1 through S9). In addition, a salt layer was introduced, which was identified in the coincident MCS record [*Keen and Potter*, 1995b]. Velocities within the sediments range from 1.8 to 5.4 km/s. The sedimentary cover has a maximum thickness of 15 km at 128 km in the Scotian Basin. At the shelf break, the sediment thickness is 12.5 km and gradually thins seaward to a value of 3 km at the southeastern end of the line in the Sohm Abyssal Plain. The minimum thickness of the sediments is 1 km between 10 and 20 km. At the northwestern end of the line around OBS 19, the sediments thicken slightly as the Orpheus Graben is approached.

[21] The continental crust has a maximum thickness of 36 km and is divided into upper, middle, and lower crust with velocities from 5.7 to 6.0 km/s, from 6.3 to 6.4 km/s, and from 6.7 to 6.9 km/s, respectively. Moho depth is fairly constant around 37 km, but it shallows rapidly to 27 km between 45 and 100 km coinciding with the thickening of the sediments in the Scotian Basin. Seaward of 100 km, the

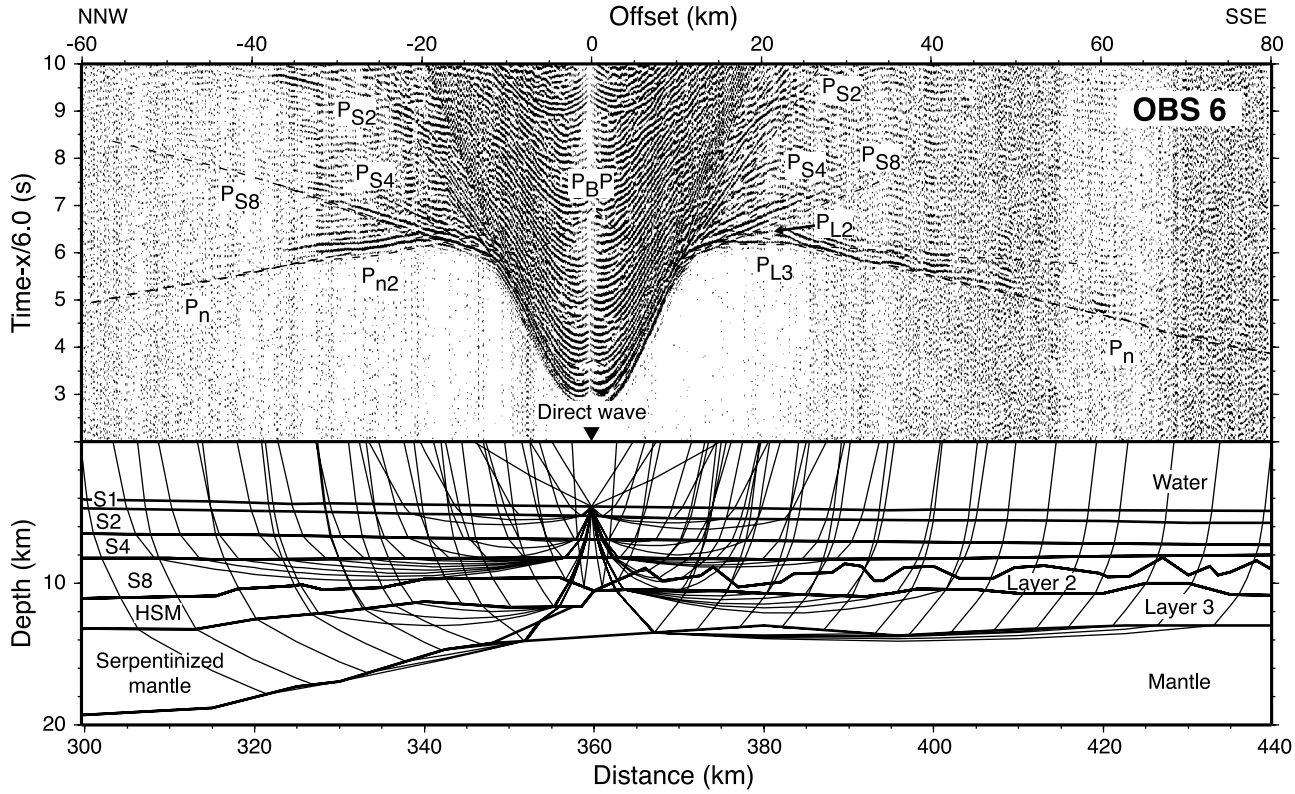

Figure 6. (top) Record section with computed travel times and (bottom) ray path diagram for the vertical geophone of OBS 6. Horizontal scale in the record section is shot-receiver distance (offset), and the vertical scale is the travel time using a reduction velocity of 6.0 km/s. Triangle indicates the receiver location. See text for description of phases and processing. The horizontal scale of the ray path diagram is distance along the velocity model (Figure 9). Abbreviations are S1 to S8, sediment layers; HSM, highly serpentinized mantle; L2 and L3, oceanic crustal layers 2 and 3.

crustal thinning is more gradual and over the next 130 km the crustal thickness decreases from 15 to 3 km. The middle crust disappears close to the hinge zone at 80 km, which is also indicated by the coincident MCS data of GSC line 89-1 [*Keen and Potter*, 1995b, Figure 2], where two zones of midcrustal reflectivity merge at shot point 4800. Upper and lower crust continue up to 230 km. Farther seaward there is no more evidence for lower crustal velocities. However, a ~3-km-thin sliver of what is interpreted to be continental crust (see discussion below) with velocities of 5.4 km/s continues for another 50 km.

[22] In the transition zone, a 4.5- to 5.5-km-thick lower layer with velocities ranging from 7.2 to 7.6 km/s is found (Figure 9), which extends over a 145-km-wide zone. To the SE, where the thin sliver of overlying continental crust has disappeared, a 2-km-thick layer with a velocity of 5.1 km/s covers the lower transitional layer. The maximum thickness of the two layers in the transition zone is 8 km. Normal mantle velocities of 8.0 km/s are encountered below a depth of ~19 km. The composition of the transition zone will be discussed later.

[23] Seaward of 358 km a 3- to 5-km-thick oceanic crust is encountered coinciding with a more variable basement relief (Figure 9). Velocities within the upper layer (oceanic layer 2) are 4.6–5.0 km/s, lower crustal velocities were modeled with 6.4–6.55 km/s (oceanic layer 3). The thickness of layer 2 varies generally between 1 and 2 km with no distinct reflections between layers 2 and 3, indicating a transitional gradient zone rather than a sharp velocity discontinuity. Moho depth is ~13 km.

4.2. Error Analysis

[24] The formal error analysis for individual phases is summarized in Table 1. The normalized χ^2 in Table 1 is based on assigned pick uncertainties of 30–200 ms depending on the quality of each individual travel time pick. Pick uncertainties are indicated in Figures 7 and 8. The model is generally well constrained with a total RMS misfit of 103 ms between calculated and picked travel times. The normalized χ^2 of 1.3 is close to the optimum value of 1.0.

[25] To estimate the resolution of the velocity model, the range of permissible variations of the model was analyzed. Outside the region of sediment layer S9, depths to basement and Moho are estimated to be accurate within 1 km. Velocities can be changed by ±0.1 km/s without compromising the fit of the observed and calculated travel times. Some areas are less constrained, such as the upper continental crust seaward of 80 km and the lower continental crust, which is sampled more by reflections (P_mP) than by refractions (P_{c3}). The velocity uncertainty for these layers is estimated to be 0.2 km/s. The same error applies to oceanic layer 2, where only short refraction branches can be correlated.

[26] While the overall resolution of the velocity model is good as just discussed, there is one region with a reduced

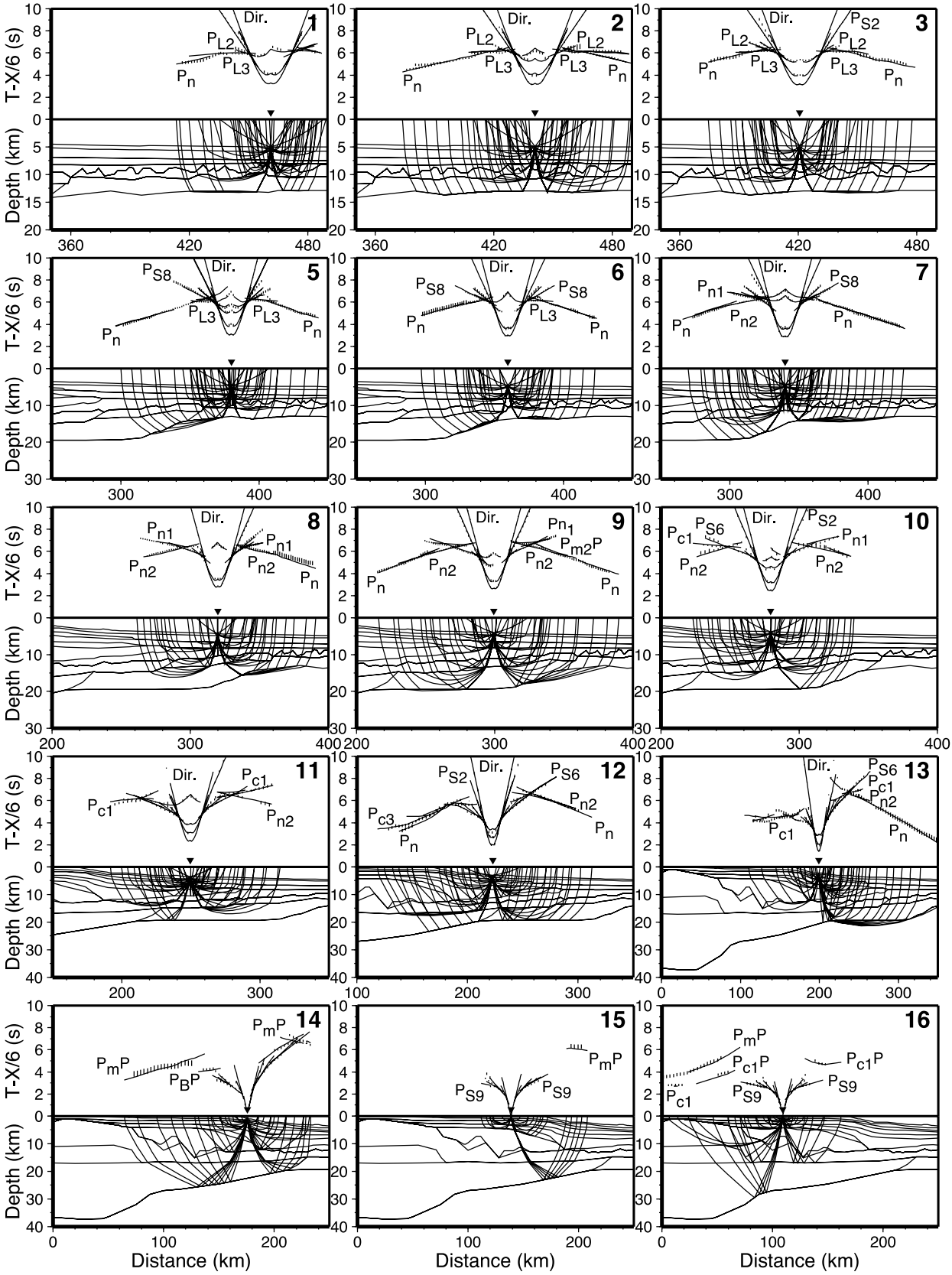

Figure 7. Comparison of observed and calculated travel times for OBS 1–16, shown together with the corresponding ray paths. Observed data are indicated by vertical bars, with heights representing pick uncertainty; calculated data are indicated by solid lines. Triangles mark the receiver locations. Horizontal scale is the model position; a reduction velocity of 6.0 km/s has been applied for the travel times. Abbreviation "Dir." is the direct wave.

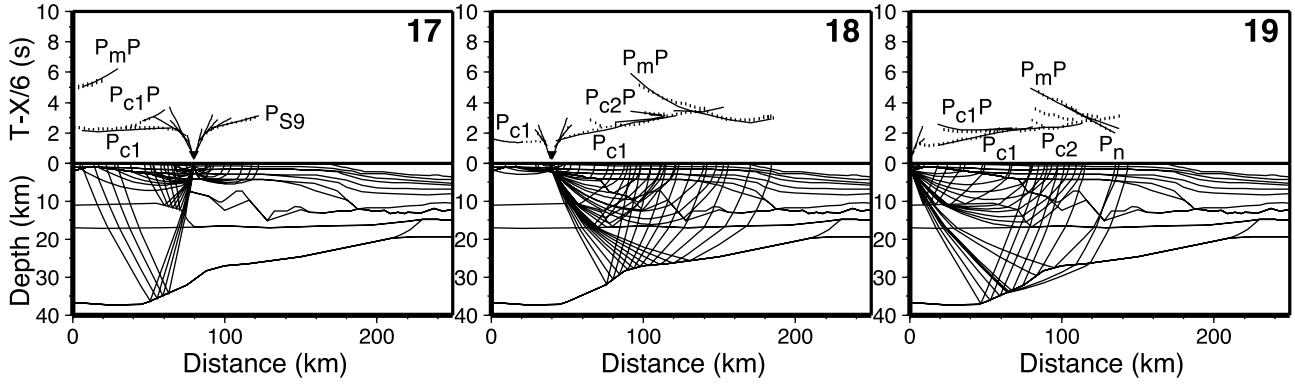

Figure 8. Same as Figure 7 for OBS 17–19.

resolution that needs some discussion. This is sediment layer S9 and the underlying salt units (Figure 9). As pointed out above in section 3.3, there is evidence for a low-velocity zone within unit S9 and the velocity structure of the layer can therefore not be resolved other than in the uppermost section. The uncertainty in velocity in layer S9 also has some influence on the basement depth between 72 and 186 km, since the geometry of the basement was largely determined by its two-way travel time in the MCS record section [*Keen and Potter*, 1995b]. Hence the conversion from two-way travel time to depth can be erroneous if a wrong velocity is used in layer S9. To estimate the possible error in basement depth in this region, we assume a velocity of 4.6 km/s for the lower part instead of the average of 5.3 km/s used in the velocity model (Figure 9). A velocity of 4.6 km/s is for example found at basement level in layer S8. The maximum deviation would occur where layer S9 is thickest (10.5 km). Using these parameters, the basement depth is accurate to within 1.5 km. Deeper layer boundaries beneath S9 are affected by this reduced resolution as well. Thus the error in Moho depth between 80 and 180 km could be as large as 2.5 km.

4.3. Gravity Modeling

[27] Two-dimensional gravity modeling (algorithm of *Talwani et al.* [1959]) was performed along line 1 to verify how consistent the velocity model is with the gravity data. The data used in the model (Figure 10) are satellite-derived free-air gravity anomalies [*Sandwell and Smith*, 1997]. The initial density model was derived from conversion of *P* wave velocities to density using the Nafe-Drake curve [*Ludwig et al.*, 1970] that is approximated by

$$\rho = -0.00283v^4 + 0.0704v^3 - 0.598v^2 + 2.23v - 0.7 \qquad (1)$$

with ρ the density in g/cm^3 and v the *P* wave velocity in km/s. The only modification to this density model was applied to the mantle, where a lateral variation was introduced. For the subcontinental mantle and for most of the mantle in the transition zone a density of 3.33 g/cm^3 was used, whereas farther seaward the density was reduced to 3.31 g/cm^3.

[28] With this adjustment, most features of the gravity signature are matched by the given density model (Figure 10). However, three regions also show a misfit between observed and calculated gravity of up to 40 mGal. The misfit at the northwestern end of the line is attributed to effects associated with the Orpheus Graben just to the north of line 1 (Figure 11b). The associated sediment basin and shallowing of the Moho can be seen on MCS line 86-5B [*Marillier et al.*, 1989]. These structures are not incorporated in the density model and explain the misfit between 0 and 50 km.

[29] The position and amplitude of the slope anomaly are well modeled (Figure 10) although the predicted anomaly between 100 km and the slope anomaly at 150 km is overestimated. In this zone, the lithostatic pressure at a depth of 40 km is calculated to be elevated to values of up to 1136 MPa, compared to an average of 1117 MPa for the entire line. Some of the misfit between observed and calculated density in this region can probably be attributed to the reduced resolution of velocity and layer boundaries in layer S9 as previously discussed.

[30] The last zone with an increased misfit between observed and calculated density is located between 190 and 220 km (Figure 10). The lithostatic pressure of the density model in this region is similar to the zone farther seaward. Instead of an erroneous density model, we assume that the reason for the misfit is rather related to three-dimensional effects at the continental slope. Figure 11b indicates that this zone with misfit (close to OBS 13) is located at the edge of a canyon wall, which is incised some 20 km landward. The expected three-dimensional complexity cannot be treated properly by the two-dimensional gravity model.

4.4. Regional Comparison of Results

[31] Only few refraction seismic experiments have been carried out off Nova Scotia for comparison with our results. There are two lines on the shelf that run parallel to the coast of Nova Scotia. This is line A of *Barrett et al.* [1964], which is almost identical to the more recent line 99-1 (Figure 1) [*Salisbury and Jackson*, 2003]. *Barrett et al.* [1964] determined a crustal thickness of 34 km, similar to the 36 to 37 km observed by *Salisbury and Jackson* [2003], who in addition noted that the Moho is basically flat along the line. This suggests that the 36-km-thick crust at the northern end of line 1 represents unstretched crust. Upper crustal velocities within the Meguma terrane are between 5.5 and 5.7 km/s [*Salisbury and Jackson*, 2003], which is similar to the 5.7 km/s observed on line 1.

[32] Line 78-5 [*Keen and Cordsen*, 1981] crosses line 1 at the position of OBS 15 (Figure 2). Depth to basement along line 78-5 is 16 km in the west and 10 km in the east, while the Moho rises from 30 to 26 km [*Keen and Cordsen*,

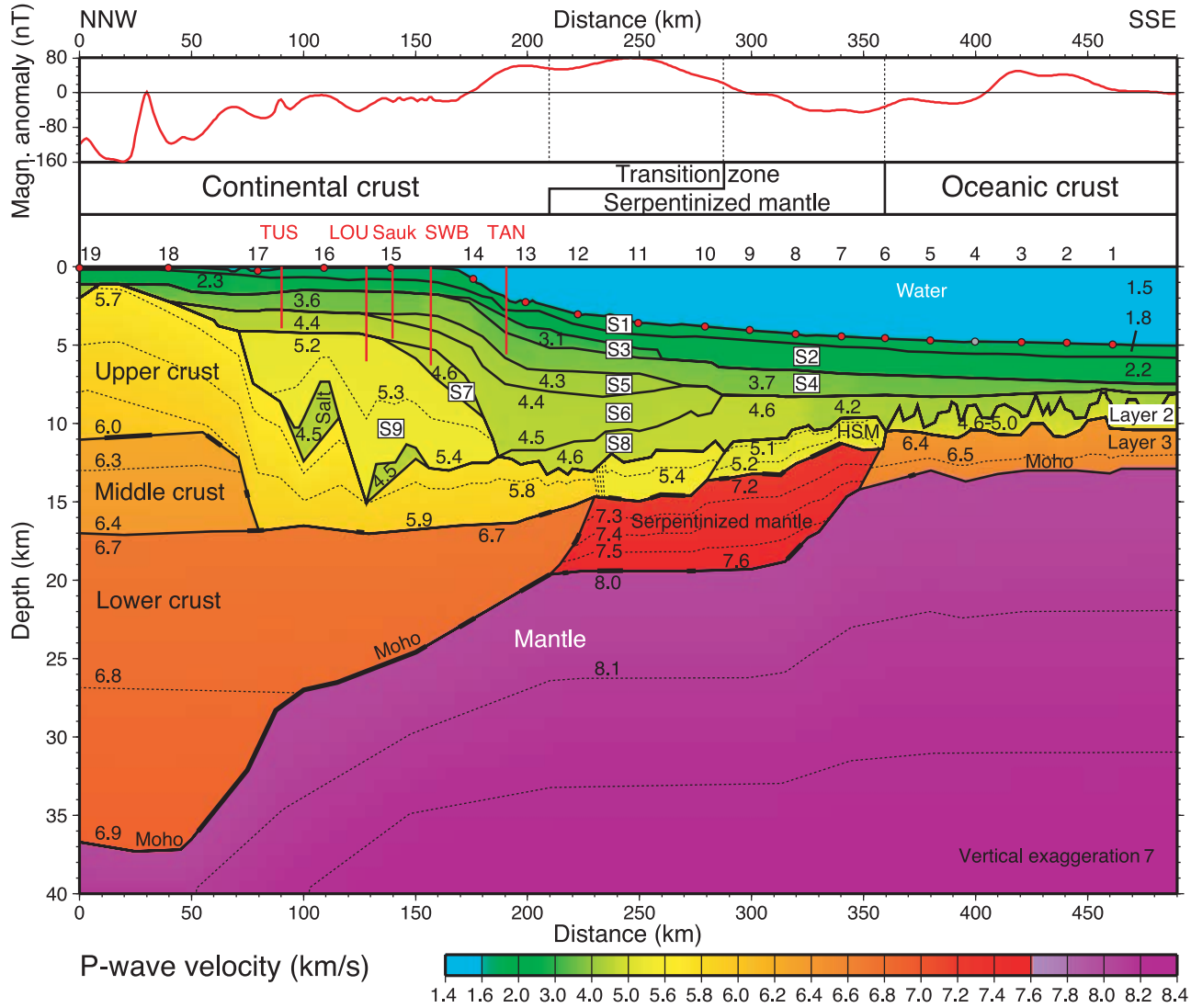

Figure 9. (bottom) *P* wave velocity model with a contour interval (dashed lines) of 0.1 km/s between 5.1 and 8.2 km/s. Numbers indicate velocity in km/s. Layer boundaries constrained by reflections are drawn with bold solid lines. Red circles mark the location of OBS used for the modeling; gray circles show the location of OBS with no data recovery. Station numbers are indicated above the velocity model. S1 through S9 are sediment layers 1 through 9. Vertical red lines show the location of deep exploration wells and their penetration in the vicinity of line 1 (TUS, Tuscarora D-61; LOU, Louisbourg J-47; Sauk, Sauk A-57; SWB, SW Banquereau F-34; TAN, Tantallon M-41). (top) Magnetic anomalies taken from *Oakey and Dehler* [2004]. Abbreviation HSM is highly serpentinized mantle.

1981]. The crust was modeled as one major layer with a velocity of 6.3 km/s. In comparison, at the cross point with line 78-5, line 1 is divided in two layers with velocities around 5.8 and 6.7 km/s, which gives a similar average crustal velocity than the 6.3 km/s observed on line 78-5. Depth to basement (14 km) and Moho (25 km) on line 1 are slightly less than on line 78-5 but are in general agreement.

5. Discussion

5.1. Character of Ocean-Continent Transition

[33] In terms of basement characterization, the new results of the wide-angle seismic data improve and modify some of the interpretations that were given earlier by *Keen and Potter* [1995b] based on the coincident MCS line 89-1. The new data suggest that the continent-ocean boundary is located ~70 km farther seaward than previously thought. In addition, the velocity model also helps to define the character of the transition zone. However, since seismic velocities of continental and oceanic crust overlap with those of serpentinized mantle, it is important to understand the possible ambiguities of the velocity model. Therefore we want to discuss the possible composition of the transition zone in some detail and make the case for our preferred model, in which most of the transition zone is serpentinized mantle.

5.1.1. Lateral Changes Within Upper Layer in Transition Zone

[34] The transition zone in the velocity model (Figure 9) extends from 210 to 360 km and consists of a lower layer

Table 1. Number of Observations (n), RMS Misfit Between Calculated and Picked Travel Times (t_{RMS}), and Normalized χ^2 for Individual Phases

Phase	n	t_{RMS}, s	χ^2
Direct wave	939	0.035	0.837
P_{S1}	59	0.091	1.820
$P_{S1}P$	101	0.102	1.399
P_{S2}	649	0.073	0.865
$P_{S2}P$	173	0.144	3.202
P_{S3}	86	0.089	0.815
P_{S4}	424	0.083	0.998
$P_{S4}P$	46	0.094	1.389
P_{S5}	255	0.093	1.559
P_{S6}	357	0.098	1.462
$P_{S6}P$	138	0.084	1.462
$P_{S7}P$	21	0.135	1.900
P_{S8}	374	0.053	0.489
P_{S9}	131	0.074	0.794
P_BP	93	0.110	1.357
P_{c1}	584	0.086	1.012
$P_{c1}P$	114	0.112	1.276
P_{c2}	102	0.083	0.697
$P_{c2}P$	20	0.062	0.411
P_{c3}	69	0.066	0.310
P_{L2}	64	0.104	1.098
P_{L3}	221	0.075	0.988
P_mP	573	0.224	3.981
P_{n1}	118	0.081	0.997
$P_{m1}P$	124	0.126	3.769
P_{n2}	391	0.100	1.939
$P_{m2}P$	65	0.088	0.927
P_n	1154	0.095	0.534
All phases	7445	0.103	1.299

with a velocity of 7.2–7.6 km/s, overlain by a layer with velocities of 5.4 km/s in the northwest and 5.1 km/s in the southeast. The lateral velocity variation within the upper layer is close to the limit of the resolution, and hence it may seem arbitrary to interpret the basement in the NW differently than the basement in the SE. To support our interpretation of two laterally distinguishable units, we first want to refer to the coincident MCS data along line 89-1 [*Keen and Potter*, 1995b], in which the basement reflection type changes around 285 km (label "C" in Figure 12). Seaward a strong basement reflector is observed, while the basement reflection landward is much weaker and exhibits more topography. This boundary coincides approximately with the seaward limit of the salt diapirs (Figure 12) and led *Keen and Potter* [1995b] to the interpretation that this is the location of the continent-ocean boundary. However, it remains possible that the change of the seismic character of the basement is not real but related to the disappearance of the overlying salt.

[35] Additional support for two different basement types in the transition zone comes from the magnetic data (Figure 9). Landward of 297 km (OBS 9), the magnetic anomaly in the transition zone is positive (up to 80 nT), while the anomalies are negative farther seaward (−43 nT). Unless the positive anomalies are associated with some sedimentary layers (e.g., layer S6, which disappears at a similar position at 287 km), this lateral variation should reflect a change within the underlying basement. In summary, even though the change in basement velocity at 285 km from 5.4 to 5.1 km/s is close

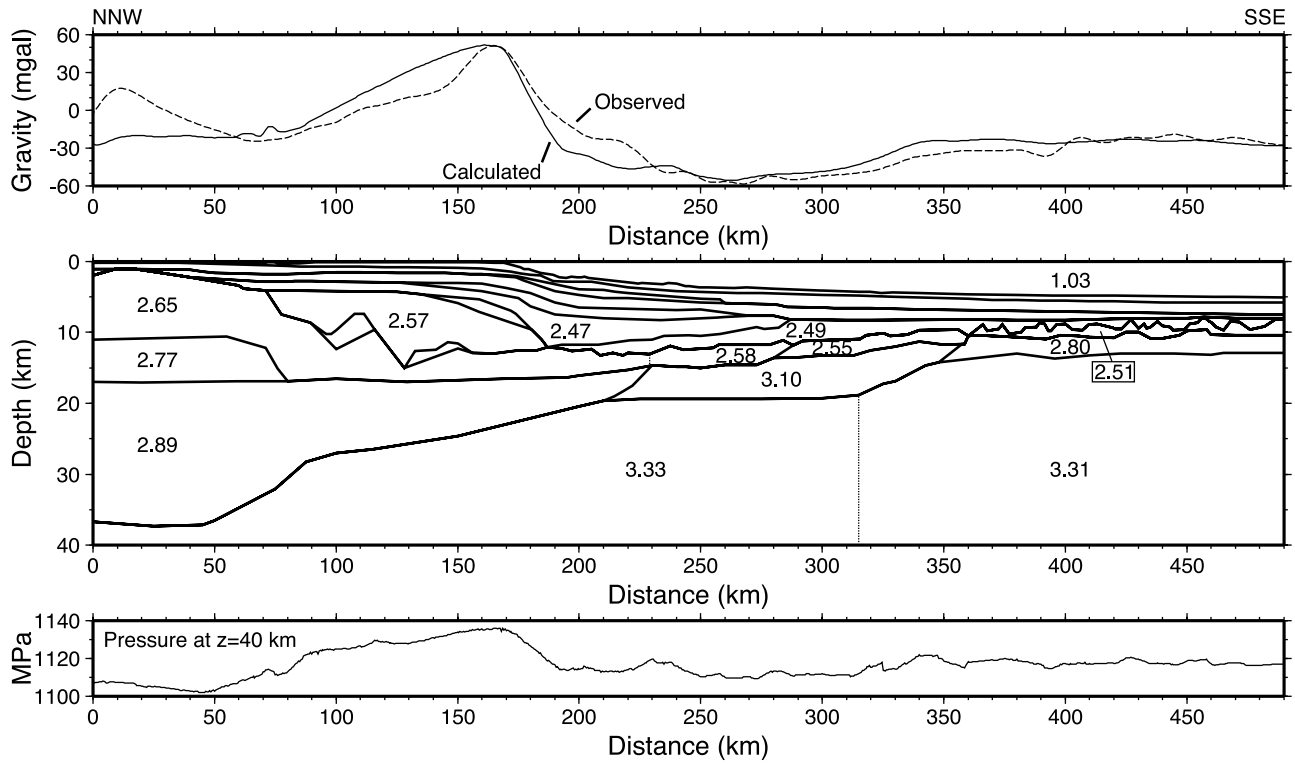

Figure 10. Two-dimensional gravity modeling for line 1. The P wave velocity model (Figure 9) was converted to density using the velocity-density relationship of *Ludwig et al.* [1970] with some modification to the densities in the mantle. (middle) Densities in the model, given in g/cm^3. (top) Observed and calculated gravity anomalies, by dashed and solid lines, respectively. (bottom) Lithostatic pressure at the base of the model at a depth of 40 km shown as solid line.

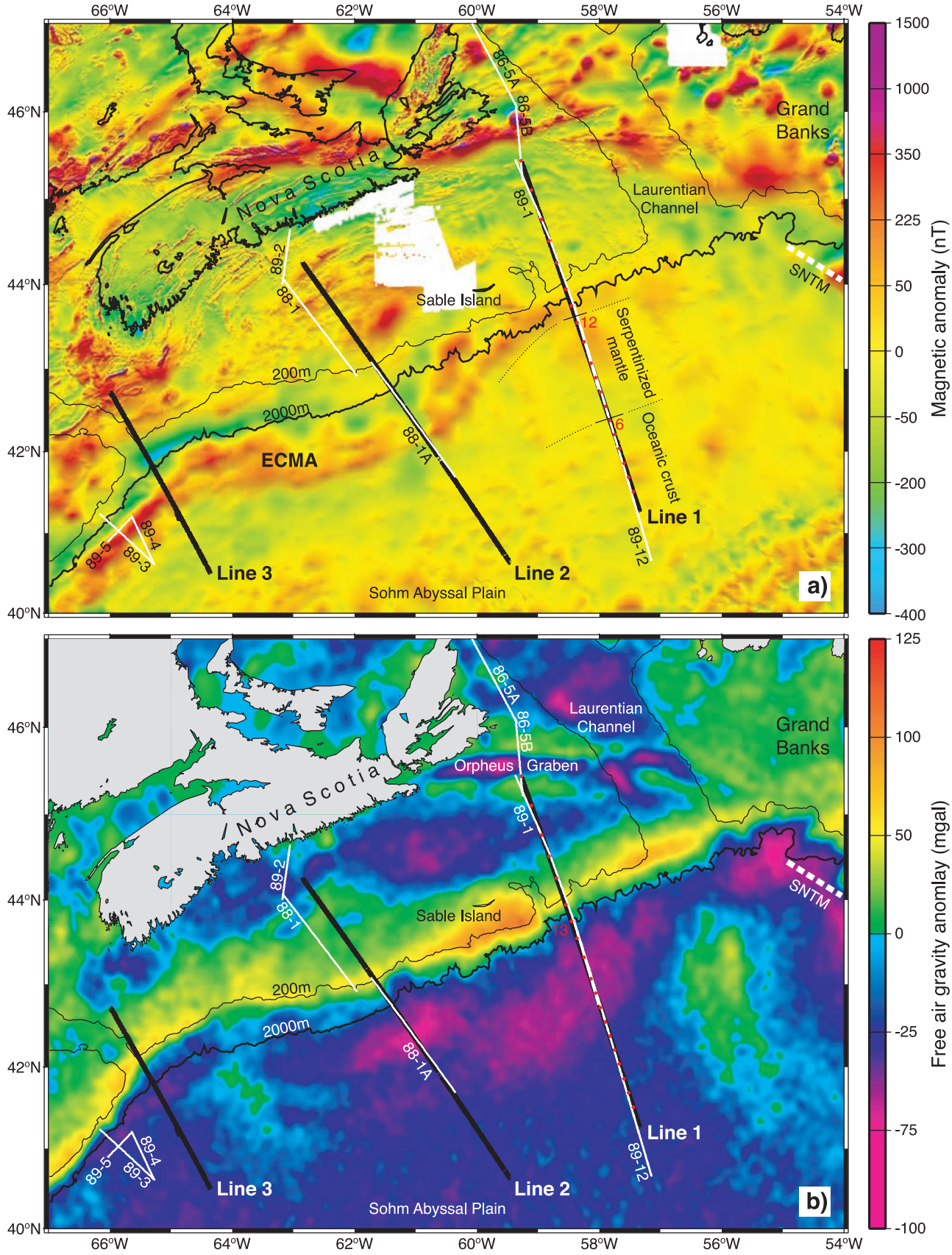
66°W
64°W
62°W
60°W
58°W
56°W
54°W
46°N
44°N
42°N
40°N
Nova Scotia
Grand Banks
Laurentian Channel
SNTM
Sable Island
Serpentinized mantle
Oceanic crust
200m
2000m
ECMA
Line 1
Line 2
Line 3
Sohm Abyssal Plain
Orpheus Graben
86-5A
86-5B
89-1
89-2
88-1
88-1A
89-12
89-5
89-4
89-3
12
6
13
a)
b)
Magnetic anomaly (nT)
1500
1000
350
225
50
0
-50
-200
-300
-400
Free air gravity anomlay (mgal)
125
100
50
0
-25
-75
-100

Figure 11

to the limit of seismic resolution there is evidence that the basement character changes at this position (layer thickness, reflection characteristics, magnetic signal, and correlation with seaward limit of salt diapirs).

5.1.2. Upper Layer in Northwestern Transition Zone

[36] The basement in the transition zone up to 285 km is thought to be continental in character. This interpretation is based on the termination of the layer close to the seaward limit of the salt diapirs (Figure 12). Unless the salt has migrated seaward up to 50 km, the underlying basement should be continental because evaporites form in shallow water environments, where oceanic crust and mantle rocks are normally not encountered for isostatic reasons.

[37] On the basis of a recent reinterpretation of MCS line 89-1, *Sahabi et al.* [2004] propose that the salt is not in its original position. They place the continent-ocean boundary about 60 km closer to the continent, which is more consistent with their plate-kinematic reconstruction. However, this would require the southeastern part of the transition zone in our velocity model (Figure 9) to be of oceanic character, which is not compatible with the obtained *P* wave velocities. The other implication of the interpretation of *Sahabi et al.* [2004] is that the initiation of seafloor spreading in the Central Atlantic started some 20 Ma earlier than previously thought (175 Ma [*Klitgord and Schouten*, 1986]). However, we do not want to dismiss the possibility that the salt has migrated. Analysis of modern two-dimensional seismic data by *Shimeld* [2004] provides some evidence for salt migration at the northeastern Nova Scotia margin. If the salt has migrated, it could still lie on thinned continental crust, or, alternatively, on serpentinized mantle. We dismiss a location on oceanic crust due to the incompatible velocity structure. Our preferred model is the one where the salt is located on continental crust because this model can best explain the lateral variations in basement character that occur at the seaward limit of the salt.

[38] Velocities of 5.4 km/s in the 3-km-thick continental crust between 230 and 285 km are lower than those found elsewhere in the upper continental crust (5.7–6.0 km/s). This reduction in velocity is attributed to alterations and fracturing associated with the extreme thinning of the crust. The thinning of the crust from 36 to 3 km occurs over a 180-km-wide zone and the crustal stretching factor β is $\sim$12.

5.1.3. Lower Layer in Transition Zone

[39] The lower layer in the transition zone between 210 and 360 km has velocities between 7.2 and 7.6 km/s (Figure 9), which are interpreted as partially serpentinized mantle but could as well fit velocities encountered in magmatic underplated layers. Farther to the southwest, the Nova Scotia margin is volcanic in character as indicated by seaward dipping reflectors (SDR) [*Keen and Potter*, 1995a] and such margins are generally also characterized by a high-velocity igneous underplated layer [e.g., *Holbrook et al.*, 1994b]. Hence, to properly characterize the along-strike variations of the Nova Scotia margin, it is essential to distinguish between the two possible explanations for the high-velocity layer. The absence of SDRs on the coincident MCS line 89-1 alone is not sufficient to dismiss the possibility of magmatic underplating because SDRs could be masked by the overlying salt or by other complexities (e.g., low signal-to-noise ratio or multiples) due to the thick sediments in the Scotian Basin.

[40] We compare the velocity model for line 1 (Figure 9) with data from volcanic margins with high-velocity igneous crustal layers. Volcanic margins like at the U.S. East Coast [*Sheridan et al.*, 1993; *Holbrook et al.*, 1994a, 1994b] and eastern Greenland [*Korenaga et al.*, 2000; *Holbrook et al.*, 2001; *Hopper et al.*, 2003] are characterized by up to 25-km-thick igneous crust, with the lower high-velocity (7.0–7.5 km/s) layer 12–15 km thick. This thick igneous crust grades laterally into normal thickness ($\sim$7 km) oceanic crust. The high-velocity layer on line 1 has a maximum thickness of only 6 km. If the overlying basement layer is included, the maximum thickness is 8 km (Figure 9). That is considerably less than indicated by observations from the volcanic margins mentioned above. However, since the Nova Scotia margin trends gradually from a volcanic margin in the south to a magma-starved margin in the north, we would not necessarily expect igneous crust of similar thickness as at the U.S. East Coast. Somewhere along the margin we would expect a volcanic weld at the ocean-continent transition that decreases in size to the north.

[41] Stronger support against a magmatic origin of the high-velocity zone on line 1 comes from the sharp lateral velocity change that occurs between the high-velocity zone and the lower oceanic crust. There is no gradual velocity decrease as observed at the U.S. East Coast [*Holbrook et al.*, 1994a, 1994b]. Instead, landward dipping reflectivity (reflector "E" in Figure 13) in the zone where the velocities change laterally from $\sim$7.3 to 6.5 km/s indicate a sharp contact. It also would be difficult to explain a volcanic margin with excessive magmatism that suddenly turns into oceanic crust with a thickness of only 4 km or less. This indicates magma starvation rather than ample magma supply. Hence we suggest that the high-velocity layer in the transition zone is partially serpentinized mantle. The depth below basement down to which serpentinization occurs is 8 km. This value fits well with other nonvolcanic margins where mantle serpentinization is observed in the transition zone (e.g., 7 km off Newfoundland [*Funck et al.*, 2003] and Labrador [*Chian et al.*, 1995b]). The line of *Chian et al.* [1995b] shows remarkable similarities to line 1. They have an 80-km-wide transition zone with a 1.5-km-thick upper layer (4.8 km/s) and a 4- to 5-km-thick lower layer (6.4–7.7 km/s). For the lower layer, *Chian et al.* [1995b] favor a

Figure 11. (a) Magnetic anomaly map and (b) free-air gravity anomaly map. Magnetic data are taken from *Oakey and Dehler* [2004], and gravity data are taken from *Sandwell and Smith* [1997]. Bold solid lines show the shot lines of the SMART experiment with red circles indicating the location of OBS along line 1. Some station numbers are annotated in red for reference. Other reflection seismic lines in the area are shown as white lines (see Figure 1 for references). The 200-m and 2000-m depth contours of the bathymetry are drawn as solid lines, the location of the southeast Newfoundland transform margin (SNTM) is indicated by a bold dashed white line. The shading of the magnetic anomalies is by illumination from the east. The interpreted zone with serpentinized mantle is outlined by a dashed line.

serpentinized peridotite origin, while they are not conclusive about the composition of the upper layer.

[42] At this time it might be worthwhile to consider how much melt could have been generated during rifting using the model of *Bown and White* [1995], in which the melt is produced by mantle decompression during uniform pure shear extension of continental lithosphere. The maximum stretching factor β along line 1 is 12. With the rifting

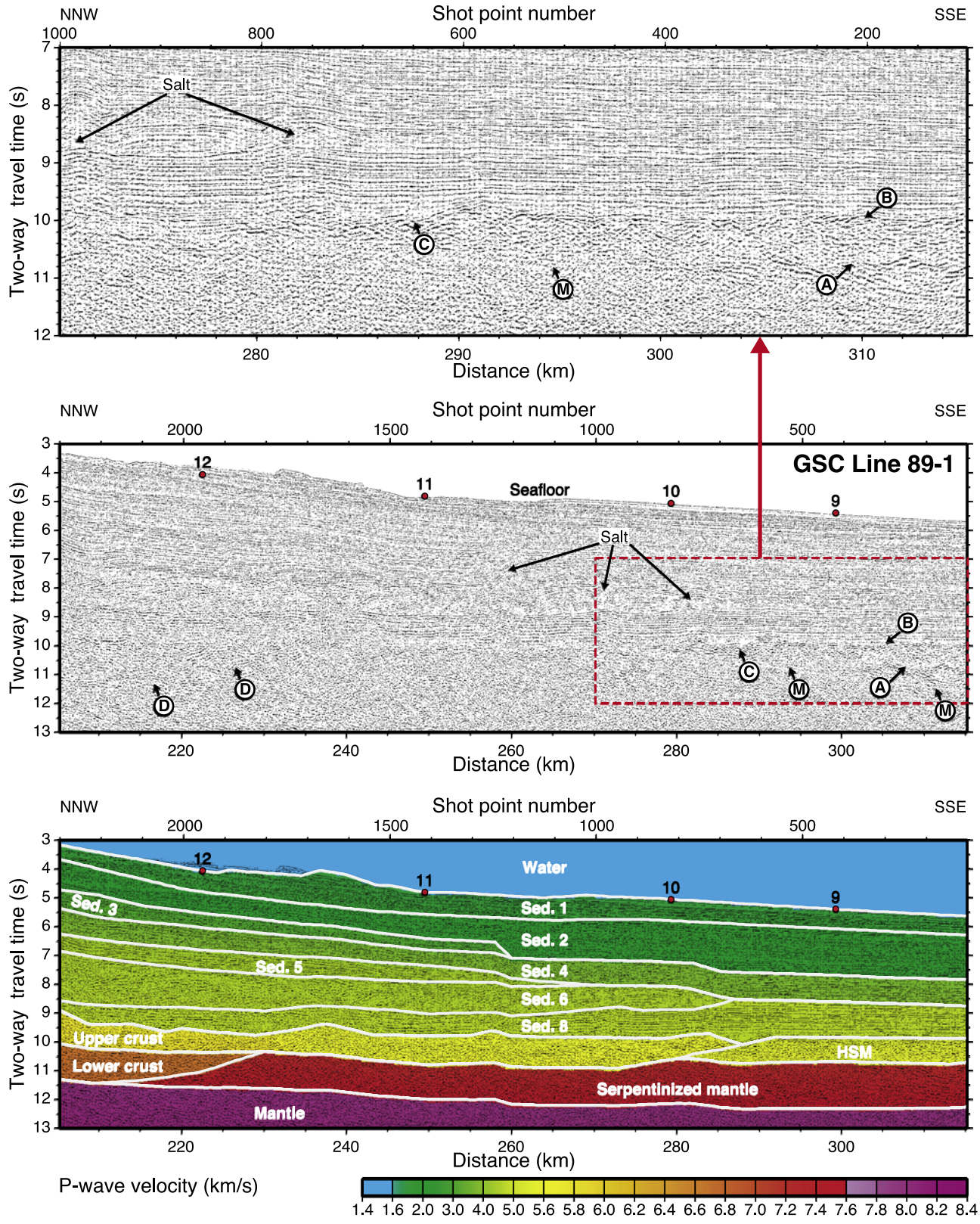

Figure 12

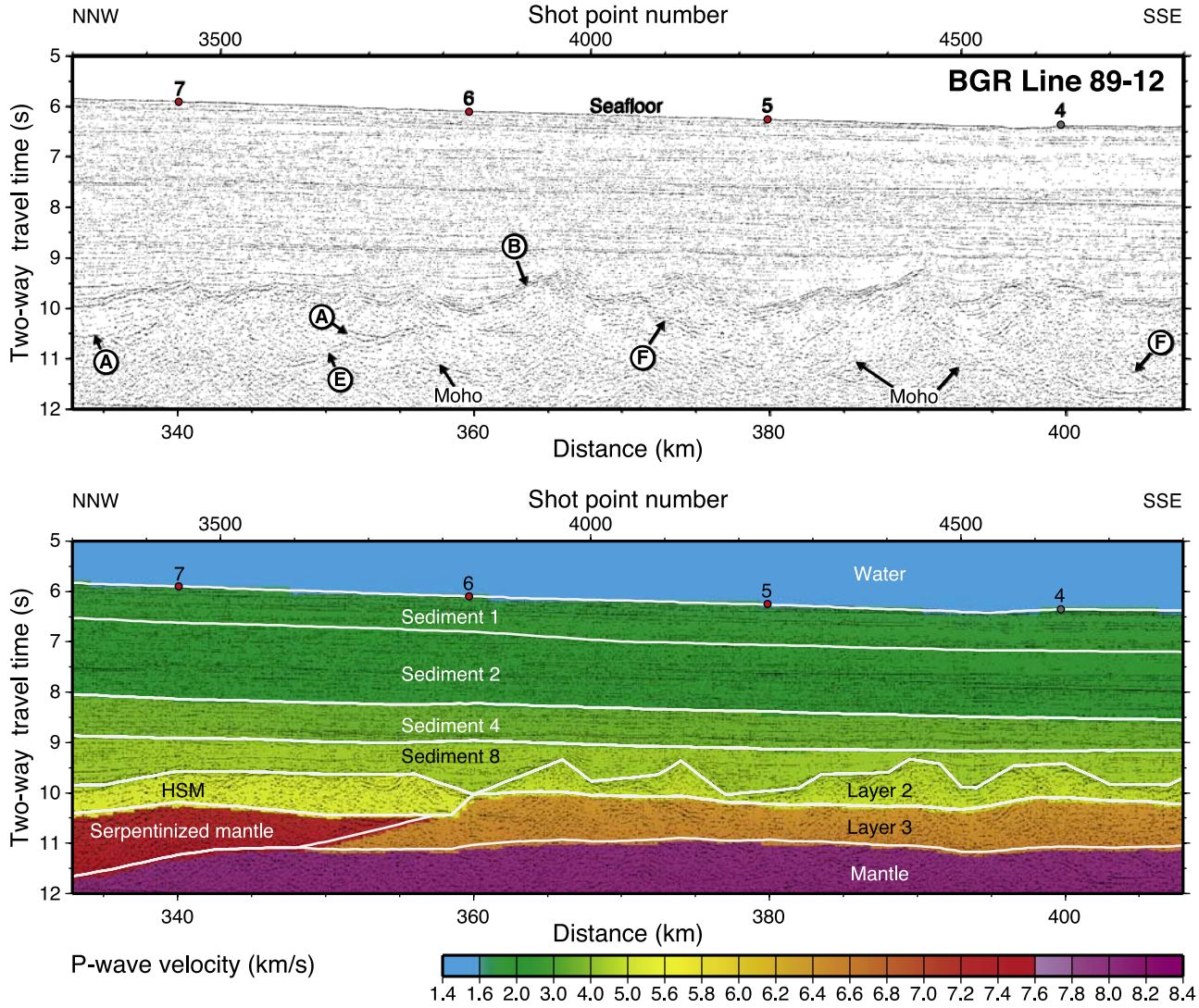

Figure 13. (top) Part of record section of MCS line 89-12 (data courtesy German Federal Agency of Geosciences and Natural Resources, BGR) and (bottom) the same record section shown together with the velocity model (Figure 9) converted to two-way travel time and with the layer boundaries drawn as white lines. The horizontal scale is distance along the velocity model (Figure 9). Red circles mark the location of OBS used for the velocity modeling, a gray circle shows the location of OBS 4 with no data recovery. Features marked by letters are A, reflector between highly and partially serpentinized mantle; B, basement; E, landward dipping reflector at the transition from serpentinized mantle to oceanic crust; F, faults. Abbreviation HSM is highly serpentinized mantle. The MCS data were recorded on a 60-channel, 3-km-long streamer. Processing includes stack and a phase shift migration.

Figure 12. (middle) Part of record section of MCS line 89-1 [*Keen and Potter*, 1995b] and (bottom) the same record section shown together with the velocity model (Figure 9) converted to two-way travel time and with the layer boundaries drawn as white lines. The dashed red line is indicating the area of the record section shown at the top. The horizontal scale is distance along the velocity model (Figure 9). Red circles mark the location of OBS. Note that there is a slight discrepancy between the seafloor depth in the MCS data and in the velocity model northwest of 250 km. This is due to an offset of up to 3 km between the MCS line and the refraction seismic line. Features marked by letters are A, reflector between highly and partially serpentinized mantle; B, basement; C, seaward limit of the thinned continental crust; D, dipping reflectors between continental crust and serpentinized mantle; and M, multiple seismic energy. Abbreviations are S1 to S8, sediment layers; HSM, highly serpentinized mantle. The MCS data were recorded by a 120-channel, 3-km-long streamer. Processing includes stack and a phase shift migration.

starting at ~230 Ma [*Welsink et al.*, 1989] and lasting until 175 Ma [*Klitgord and Schouten*, 1986], no melt would be generated according to *Bown and White* [1995] because the long duration of rifting is sufficient to cool the asthenospheric mantle. Even if seafloor spreading started already at 195 Ma as suggested by *Sahabi et al.* [2004], no melt would be expected. Hence our interpretation of the transition zone as serpentinized mantle is consistent with the melt generation model of *Bown and White* [1995].

5.1.4. Upper Layer in Southeastern Transition Zone

[43] The last remaining layer in the transition zone to be discussed is the 2-km-thick layer overlying the partially serpentinized mantle between 285 and 360 km (Figure 9). In principal, the velocities of 5.1–5.2 km/s can correspond to continental or oceanic crust, or to serpentinized mantle. A continental origin does not appear very likely. *Keen and Potter* [1995b] show that the basement in this zone is rather flat (see also Figures 12 and 13), whereas the continental basement farther landward exhibits greater topography. Thinned continental crust is expected to be characterized by a series of fault-bounded blocks, rather than by a subdued basement relief [*Pickup et al.*, 1996]. In addition, the basement relief is not only rather flat, but also the layer thickness of 2 km is very constant over a 75-km-wide zone. More variations would be expected in such a wide zone of extremely thinned and brittle upper crust. Finally, the basement in this area is overlain by the flat lying postrift sediments of the Sohm Abyssal Plain [*Ebinger and Tucholke*, 1988]. In summary, there is no evidence that the basement here is thinned continental crust.

[44] Off the south side of Flemish Cap on the Newfoundland margin, a 60-km-wide zone of partially serpentinized mantle is overlain by 1- to 4-km-thick oceanic crust [*Funck et al.*, 2003; *Hopper et al.*, 2004]. The thin oceanic crust is highly tectonized and is explained by ultraslow seafloor spreading with a low and variable magma supply. With a more sporadic magma supply, it would be difficult to create a layer with a fairly constant thickness as observed for the upper basement layer between 285 and 360 km (Figure 9).

[45] The remaining possibility is that the upper basement layer between 285 and 360 km (Figure 9) is serpentinized mantle. This interpretation can also explain why the layer has a nearly constant thickness of 2 km over its width of 75 km. Rather than being a tectonically or magmatically controlled boundary, the base of the layer is a serpentinization front, where the exhumed upper mantle changes its character from highly (85–100%) to only partially (10–25%) serpentinized mantle. The degree of serpentinization is inferred from the observed *P* wave velocities of 5.1 km/s and 7.2–7.6 km/s in the upper and lower layer, respectively, and comparison with the compilation of *Miller and Christensen* [1997]. One reason for this abrupt vertical change in the degree of serpentinization might be that the expansion of the peridotites during the serpentinization process seals the fractures and fluid paths in the rock and thus prevents seawater from penetrating deeper into the mantle. This may be controlled by the initial depth down to which faults and microcracks in the peridotite allowed a vigorous water circulation.

[46] In the southern Iberia Abyssal Plain, *Dean et al.* [2000] found a similar upper basement layer on the IAM-9 transect, ~2 km thick and with a velocity of 5.2 km/s, which they interpreted as serpentinized mantle. Drilling in the southern Iberia Abyssal Plain [*Sawyer et al.*, 1994; *Whitmarsh et al.*, 2000] has shown the widespread occurrence of exhumed upper mantle material in the transition zone.

[47] MCS data along the IAM-9 transect also show that the upper basement layer in the transition zone has a low internal reflectivity and that the top of the lower basement layer has increased reflectivity [*Pickup et al.*, 1996]. This is similar to the reflection seismic data along our line 1. The highly serpentinized mantle has a reduced reflectivity while the top of the partially serpentinized mantle is characterized by strong reflectivity along large sections (reflector "A" in Figures 12 and 13). In their interpretation of MCS line 89-1, *Keen and Potter* [1995b] assume that the basement is oceanic and compare reflector "A" (Figure 12) about 1 s below basement to similar reflections in oceanic crust found elsewhere [e.g., *Morris et al.*, 1993]. However, line 89-1 ends at 315 km, and hence *Keen and Potter* [1995b] were unaware of the much wider transition zone with the oceanic basement first starting at 360 km (Figure 9).

5.2. Oceanic Crust

[48] Seaward of 360 km, the basement is interpreted as oceanic crust (Figure 9). However, based on comparison with seismic properties of average ocean crust [*White et al.*, 1992], its layers are thinner than average. Its average total thickness is 4.0 km compared with 7.1 ± 0.8 km for normal oceanic crust; its average thickness of layer 2 is 1.3 km, compared with the global average of 2.1 ± 0.6 km; and its average thickness of layer 3 is 2.7 km, compared to a global average of 5.0 ± 0.9 km. Typical velocities within layer 3 of 6.5 km/s are slightly low compared to values of 6.7 to 7.2 km/s for average oceanic crust [*White et al.*, 1992]. However, in some instances velocities between 6.4 and 6.7 km/s have been observed at the top of layer 3 [e.g., *Henstock et al.*, 1996].

[49] Half spreading rates for the initial opening until magnetic anomaly M21 are around 20 mm/year [*Klitgord and Schouten*, 1986], although earliest anomalies might suggest a somewhat lower rate of ~16 mm/year [*Louden et al.*, 1987]. This rate is too high to relate the reduced magma production rate on line 1 to ultraslow seafloor spreading [*Dick et al.*, 2003], which creates oceanic crust with a thickness of <4 km (e.g., Mohns Ridge [*Klingelhöfer et al.*, 2000], Gakkel Ridge [*Jokat et al.*, 2003], extinct Labrador Sea spreading center [*Louden et al.*, 1996]). Extension may be a factor that contributed to the thinning of the oceanic crust on line 1, similar to observations in the Labrador Sea [*Srivastava and Keen*, 1995], where the average melt production was reduced compared to the space created by the separation of the plates resulting in tectonic extension of the crust [see *Louden et al.*, 1996]. Since faulting is observed within the oceanic crust of line 1 (Figure 13), extension may have contributed to crustal thinning. Some of the faults can be traced below reflection Moho.

[50] It remains unclear what caused the reduced magma supply on line 1. Seismic refraction data from the U.S. Atlantic margin show an oceanic crustal thickness of 7–8 km [*Holbrook et al.*, 1994a, 1994b] at the seaward end of

the line where the spreading rate is similar to SMART line 1[*Klitgord and Schouten*, 1986]. Preliminary models for SMART line 2 show a 5-km-thick oceanic crust (Y. Wu, personal communication, 2004), which is thicker than the 4 km observed on line 1 but still less than normal thickness oceanic crust. One possible assumption is that the proximity of the southeast Newfoundland transform margin (Figure 1) could have had some influence on the magma supply on line 1. Data from the transform margin off Ghana in the equatorial Atlantic show that the oceanic crust within 70 km of the margin is just 4.4 km thick [*Edwards et al.*, 1997], which is attributed to conductive loss of heat from upwelling oceanic mantle in a small basin surrounded, on at least three sides, by cold continental lithosphere. Unfortunately, the seismic line off Ghana does not extend far enough to determine the width of the thinned oceanic crust. Seismic and gravity data some 200 km farther to the west of the Ghana experiment show that the oceanic crust is abnormal over a distance of 50–70 km away from the transform margin [*Sage et al.*, 2000]. Thus there is evidence that the magma supply in the vicinity of transform margins can be reduced.

[51] In the case of SMART line 1, the distance to the southeast Newfoundland transform margin is ~350 km and it needs to be tested if the zone with thinned oceanic crust extends all the way up to the transform margin. On a line across the transform margin (line T88 in Figure 1), *Todd et al.* [1988] found 7- to 8-km-thick crust with velocities of 4.7–6.5 km/s. Although a distinct layer 3 is absent, this crust was interpreted to be oceanic in character. The data show that oceanic crust close to a transform margin can have normal thickness. However, this line across the transform margin is located on younger crust than our line 1 and it is also in the proximity of the Fogo seamounts (Figure 1), which may locally produce thicker crust. Just to the southwest of the Fogo seamounts, *Keen et al.* [1990a] estimate the crustal thickness to be between 6 and 7 km based on MCS data.

[52] No matter what caused the reduced magma supply on line 1, the low layer 3 velocity and crustal thickness of 4 km suggest a brief comparison with oceanic fracture zones, which are commonly associated with low magma production rates [*Detrick et al.*, 1993]. The velocity structure within fracture zones is quite variable as summarized by *Minshull et al.* [1998], but normal seismic layer 3 velocities (6.7–7.2 km/s) are generally absent [*Detrick et al.*, 1993]. Instead of interpreting our velocity of 6.5 km/s as within the lower limits of layer 3, it could be explained by more abnormal fracture zone-style crust. For example, velocities within the small-offset fracture zone I south of the Oceanographer fracture zone are between 6.25 and 6.55 km/s [*White et al.*, 1984].

5.3. Continental Crust

[53] The maximum crustal thickness observed on line 1 is 36 km (Figure 9). Thinning of the crust starts at ~50 km and is relatively evenly distributed between the upper/middle crust and the lower crust, even though the middle crust disappears at 80 km. The lower crust can be traced up to 230 km. Still farther seaward, a 3-km-thick layer interpreted as upper continental crust continues up to 285 km.

[54] The pinch out of the middle crust at 80 km is in the vicinity of the steep western limit of the deep sedimentary basin, suggesting a possible relation between these two features. One explanation could be that the middle crust is truncated by a rift-related normal fault. The reflection seismic record of line 89-1 [*Keen and Potter*, 1995b] does not provide a conclusive answer to this question since no basement faults are observed in this area. The data only show steeply dipping reflections near the hinge zone originating in synrift and early postrift sediments, which may mimic faults in the underlying basement [*Keen and Potter*, 1995b].

[55] Another possibility is that the truncation of the middle crust is related to preexisting structures. One obvious candidate could be the suture between the Avalon and Meguma Appalachian terranes at the northern end of line 1. Joint analysis of MCS line 89-1 [*Keen and Potter*, 1995b] and line 86-5B [*Marillier et al.*, 1989] show a major south dipping basin bounding fault at the Orpheus Graben, which intersects the Moho on our coincident line 1 (Figure 9) at 25 km. *Keen and Potter* [1995b] note that such fault systems are prevalent offshore Nova Scotia and on the Grand Banks, wherever Triassic basins occur landward of the main rift zone. The fault observed at the Orpheus Graben lies along the Paleozoic Avalon-Meguma suture [*Williams*, 1979] some 50 km to the north of the truncation of the middle crust on line 1. Hence we cannot establish a clear link between known preexisting structures and the disappearance of the middle crust.

5.4. Along-Strike Variations of Margin

[56] The velocity model for line 1 (Figure 9) shows that the northern segment of the Nova Scotia margin is nonvolcanic. One of the objectives of the SMART study was to identify along-strike variations in crustal structure in order to understand what controlled the transition from volcanic to nonvolcanic style margins off Nova Scotia. On the basis of the velocity model for SMART line 1 and available reflection seismic data, some initial observations are briefly presented here.

[57] In the southwest, SDR units were identified on MCS lines 89-3 and 89-4 [*Keen and Potter*, 1995a] in the area with a strong ECMA just 60 km to the south of SMART line 3 (Figure 11a). Hence the southern segment of the Nova Scotia margin is clearly volcanic. Just to the east of line 3, the strike of the ECMA changes from SW-NE to east-west (Figure 11a) up to SMART line 2. No SDRs are observed on MCS line 88-1A [*Keen et al.*, 1991] that runs parallel to line 2. If the SDRs are not hidden beneath salt structures of the Slope Diapiric Province, volcanic extrusives should disappear somewhere between lines 3 and 2.

[58] The magnetic anomaly map (Figure 11a) shows a good correlation with the different basement types encountered along line 1. The continental crust extends up to the weak northeastern remainder of the ECMA. Between OBS 12 and 6, rather subdued anomalies characterize the transitional crust with serpentinized mantle, which is partly overlain by thin continental crust. At the seaward end of line 1, where oceanic crust is observed, the wavelength of the anomalies becomes shorter, creating a ''speckled'' magnetic pattern. Clear magnetic lineations are first identified to the SE of line 1. The speckled pattern can be

correlated toward line 2 where it starts seaward of MCS line 88-1A.

[59] Knowledge of the basement type along MCS line 88-1A [*Keen et al.*, 1991] is ambiguous. *Keen et al.* [1991] interpreted the zone seaward of the Slope Diapiric Province (Figure 1) as possibly oceanic in character. However, they noted that several listric faults observed in this area can be explained in either a continental or oceanic context. Later, *Salisbury and Keen* [1993] argued that these faults are features within oceanic basement.

6. Conclusions

[60] The *P* wave velocity model obtained for SMART line 1 (Figure 9) constitutes a significant modification of the earlier interpretation of basement types along this segment of the Nova Scotia continental margin, which was based on MCS line 89-1 [*Keen and Potter*, 1995b]. Line 1 extends beyond line 89-1 and shows that oceanic crust is first encountered 25 km seaward of line 89-1, which moves the continent-ocean boundary some 60 km farther to the southeast compared to the earlier interpretation of *Keen and Potter* [1995b]. The crustal structure of the margin along line 1 can be divided into three zones: (1) continental crust with a full thickness of 36 km, which thins to just 3 km over a 180-km-wide zone (the sediment cover in the Scotian Basin is up to 15 km thick), (2) a 150-km-wide transition zone with partially serpentinized mantle overlain by 3-km-thick continental crust in the NW and by exhumed and highly serpentinized mantle in the SE, and (3) oceanic crust at the seaward end of the line with an average thickness of 4 km indicating a reduced magma supply.

[61] Comparison with the magnetic anomaly map (Figure 11a) shows that these three zones have distinct magnetic patterns allowing for some possible correlation along-strike the margin. This correlation suggests that the transition zone with serpentinized mantle narrows toward the SW but it remains unclear where exactly it disappears.

[62] The reduced thickness of oceanic crust on line 1 fits into the general picture that the Nova Scotia continental margin becomes progressively more nonvolcanic to the northeast. A reduced magma supply could be related to the proximity ($\sim$350 km) to the southeast Newfoundland transform margin. However, data from other transform margins [e.g., *Sage et al.*, 2000] suggest that the zone with thin oceanic crust does not extend that far from the transform margins. Hence additional data between line 1 and the transform margin are needed to causally relate the reduced oceanic crustal thickness to thermal effects associated with the proximity to the transform margin.

[63] **Acknowledgments.** We thank all individuals onboard the CCGS *Hudson* who helped to conduct the seismic experiment in a very professional manner. The experiment was funded by the Natural Science and Engineering Research Council of Canada and the Geological Survey of Canada. Danish project participation and data analysis were supported by the Danish National Research Foundation (Danmarks Grundforskningsfond). Seismic line BGR 89-12 was collected as part of a collaborative program between the Geological Survey of Canada and the German Federal Agency of Geosciences and Natural Resources (BGR). We thank Charlotte Keen, John Shimeld, and Patrick Potter for comments on the manuscript. Frauke Klingelhöfer and Harm Van Avendonk made very thoughtful suggestions that improved the manuscript. Geological Survey of Canada contribution 2003309.

References

Barr, S. M., and R. P. Raeside (1989), Tectono-stratigraphic terranes in Cape Breton Island, Nova Scotia: Implications for the configuration of the northern Appalachian orogen, *Geology*, *17*, 822–825.

Barrett, D. L., M. Berry, J. E. Blanchard, M. J. Keen, and R. E. McAllister (1964), Seismic studies on the eastern seaboard of Canada: The Atlantic coast of Nova Scotia, *Can. J. Earth Sci.*, *1*, 10–22.

Bown, J. W., and R. S. White (1995), Effect of finite extension rate on melt generation at rifted continental margins, *J. Geophys. Res.*, *100*, 18,011–18,029.

Chian, D., C. Keen, I. Reid, and K. E. Louden (1995a), Evolution of nonvolcanic rifted margins: New results from the conjugate margins of the Labrador Sea, *Geology*, *23*, 589–592.

Chian, D., K. E. Louden, and I. Reid (1995b), Crustal structure of the Labrador Sea conjugate margin and implications for the formation of nonvolcanic continental margins, *J. Geophys. Res.*, *100*, 24,239–24,253.

Dean, S. M., T. A. Minshull, R. B. Whitmarsh, and K. E. Louden (2000), Deep structure of the ocean-continent transition in the southern Iberia Abyssal Plain from seismic refraction profiles: The IAM-9 transect at 40°20′N, *J. Geophys. Res.*, *105*, 5859–5885.

Detrick, R. S., R. S. White, and G. M. Purdy (1993), Crustal structure of North Atlantic fracture zones, *Rev. Geophys.*, *31*, 439–458.

Dick, H. J., J. Lin, and H. Schouten (2003), An ultraslow-spreading class of ocean ridge, *Nature*, *426*, 405–412, doi:10.1038/nature02128.

Ebinger, C. J., and B. E. Tucholke (1988), Marine geology of Sohm Basin, Canadian Atlantic margin, *AAPG Bull.*, *72*, 1450–1468.

Edwards, R. A., R. B. Whitmarsh, and R. A. Scrutton (1997), The crustal structure across the transform continental margin off Ghana, eastern equatorial Atlantic, *J. Geophys. Res*, *102*, 747–772.

Funck, T., J. R. Hopper, H. C. Larsen, K. E. Louden, B. E. Tucholke, and W. S. Holbrook (2003), Crustal structure of the ocean-continent transition at Flemish Cap: Seismic refraction results, *J. Geophys. Res.*, *108*(B11), 2531, doi:10.1029/2003JB002434.

Gibling, M. R., R. C. Boehner, and B. R. Rust (1987), The Sydney Basin of Atlantic Canada: An upper Paleozoic strike-slip basin in a collisional setting, in *Sedimentary Basins and Basin-Forming Mechanisms*, edited by C. Beaumont and A. J. Tankard, *Mem. Can. Soc. Pet. Geol.*, *12*, 269–285.

Hall, J., F. Marillier, and S. Dehler (1998), Geophysical studies of the structure of the Appalachian orogen in the Atlantic borderlands of Canada, *Can. J. Earth Sci.*, *35*, 1205–1221.

Harry, D. L., and J. C. Bowling (1999), Inhibiting magmatism on nonvolcanic rifted margins, *Geology*, *27*, 895–898.

Henstock, T. J., R. S. White, and J. H. McBride (1996), Along-axis variability in crustal accretion at the Mid-Atlantic Ridge: Results from the OCEAN study, *J. Geophys. Res.*, *101*, 13,673–13,688.

Holbrook, W. S., and P. B. Kelemen (1993), Large igneous province on the US Atlantic margin and implications for magmatism during continental breakup, *Nature*, *364*, 433–436.

Holbrook, W. S., G. M. Purdy, R. E. Sheridan, L. Glover III, M. Talwani, and D. Hutchinson (1994a), Seismic structure of the U.S. Mid-Atlantic continental margin, *J. Geophys. Res.*, *99*, 17,871–17,891.

Holbrook, W. S., E. C. Reiter, G. M. Purdy, D. Sawyer, P. L. Stoffa, J. A. Austin, J. Oh, and J. Makris (1994b), Deep structure of the U.S. Atlantic continental margin, offshore North Carolina, from coincident ocean-bottom and multichannel seismic data, *J. Geophys. Res.*, *99*, 9155–9178.

Holbrook, W. S., et al. (2001), Mantle thermal structure and active upwelling during continental breakup in the North Atlantic, *Earth Planet. Sci., Lett.,190*, 251–266.

Hopper, J. R., T. Dahl-Jensen, W. S. Holbrook, H. C. Larsen, D. Lizarralde, J. Korenaga, G. M. Kent, and P. B. Kelemen (2003), Structure of the SE Greenland margin from seismic reflection and refraction data: Implications for nascent spreading center subsidence and asymmetric crustal accretion during North Atlantic opening, *J. Geophys. Res.*, *108*(B5), 2269, doi:10.1029/2002JB001996.

Hopper, J. R., T. Funck, B. E. Tucholke, H. C. Larsen, W. S. Holbrook, K. E. Louden, D. Shillington, and H. Lau (2004), Continental breakup and the onset of ultraslow seafloor spreading off Flemish Cap on the Newfoundland rifted margin, *Geology*, *32*(1), 93–96, doi:10.1130/G19694.1.

Jokat, W., O. Ritzmann, M. C. Schmidt-Aursch, S. Drachev, S. Gauger, and J. Snow (2003), Geophysical evidence for reduced melt production on the Arctic ultraslow Gakkel mid-ocean ridge, *Nature*, *423*, 962–965, doi:10.1038/nature01706.

Keen, C. E., and A. Cordsen (1981), Crustal structure, seismic stratigraphy, and rift processes of the continental margin off eastern Canada: Ocean bottom seismic refraction results off Nova Scotia, *Can. J. Earth Sci.*, *18*, 1523–1538.

Keen, C. E., and P. Potter (1995a), The transition from a volcanic to nonvolcanic rifted margin off eastern Canada, *Tectonics*, *14*, 359–371.

Keen, C. E., and P. Potter (1995b), Formation and evolution of the Nova Scotian rifted margin: Evidence from deep seismic reflection data, *Tectonics*, *14*, 918–932.

Keen, C. E., W. A. Kay, and W. R. Roest (1990a), Crustal anatomy of a transform continental margin, *Tectonophysics*, *173*, 527–544.

Keen, C. E., B. D. Loncarevic, I. Reid, J. Woodside, R. T. Haworth, and H. Williams (1990b), Tectonic and geophysical overview, in *The Geology of North America*, vol. I-1, *Geology of the Continental Margin of Eastern Canada*, *Geol. Can.*, no. 2, edited by M. J. Keen and G. J. Williams, pp. 31–85, Geol. Surv. of Can., Ottawa, Ont.

Keen, C. E., B. C. MacLean, and W. A. Kay (1991), A deep seismic reflection profile across the Nova Scotia continental margin, offshore eastern Canada, *Can. J. Earth Sci.*, *28*, 1112–1120.

Klingelhöfer, F., L. Géli, L. Matias, N. Steinsland, and J. Mohr (2000), Crustal structure of a super-slow spreading centre: A seismic refraction study of Mohns Ridge, 72°N, *Geophys. J. Int.*, *141*, 509–526.

Klitgord, K. D., and H. Schouten (1986), Plate kinematics of the central Atlantic, in *The Geology of North America*, vol. M, *The Western North Atlantic Region*, edited by P. R. Vogt and B. E. Tucholke, pp. 351–378, Geol. Soc. of Am., Boulder, Colo.

Korenaga, J., W. S. Holbrook, G. M. Kent, P. B. Kelemen, R. S. Detrick, H. C. Larsen, J. R. Hopper, and T. Dahl-Jensen (2000), Crustal structure of the southeast Greenland margin from joint refraction and reflection seismic tomography, *J. Geophys. Res.*, *105*, 21,591–21,614.

Louden, K. E., and D. Chian (1999), The deep structure of non-volcanic rifted continental margins, *Philos. Trans. R. Soc. London*, *Ser. A*, *357*, 767–804.

Louden, K. E., D. O. Wallace, and R. C. Courtney (1987), Heat flow and depth versus age for the northwest Atlantic Ocean: Results from the Sohm abyssal plain and implications for the Bermuda Rise, *Earth Planet. Sci. Lett.*, *83*, 109–122.

Louden, K. E., J. C. Osler, S. P. Srivastava, and C. E. Keen (1996), Formation of oceanic crust at slow spreading rates: New constraints from an extinct spreading center in the Labrador Sea, *Geology*, *24*, 771–774.

Ludwig, W. J., J. E. Nafe, and C. L. Drake (1970), Seismic refraction, in *The Sea*, vol. 4, *New Concepts of Sea Floor Evolution*, *Part I*, edited by A. E. Maxwell, pp. 53–84, Wiley-Interscience, Hoboken, N. J.

Marillier, F., C. E. Keen, G. S. Stockmal, G. Quinlan, H. Williams, S. P. Colman-Sadd, and S. J. O'Brien (1989), Crustal structure and surface zonation of the Canadian Appalachians: Implications of deep seismic reflection data, *Can. J. Earth Sci.*, *26*, 305–321.

Miller, D. J., and N. I. Christensen (1997), Seismic velocities of lower crustal and upper mantle rocks from the slow-spreading Mid-Atlantic Ridge, south of the Kane Transform zone (MARK), *Proc. Ocean Drill. Program Sci. Results*, *153*, 437–454.

Minshull, T. A., M. R. Muller, C. J. Robinson, R. S. White, and M. J. Bickle (1998), Is the oceanic Moho a serpentinization front?, in *Modern Ocean Floor Processes and the Geological Record*, edited by R. A. Mills and K. Harrison, *Spec. Publ. Geol. Soc.*, *148*, 71–80.

Morris, E., R. S. Detrick, T. A. Minshull, J. C. Mutter, R. S. White, W. Su, and P. Buhl (1993), Seismic structure of oceanic crust in the Western North Atlantic, *J. Geophys. Res.*, *98*, 13,879–13,903.

Oakey, G. N., and S. A. Dehler (2004), Atlantic Canada magnetic map series: Scotian shelf and surrounds, *Open File Rep. 1814*, Geol. Surv. of Can., Calgary, Alberta.

Pickup, S. L. B., R. B. Whitmarsh, C. M. R. Fowler, and T. J. Reston (1996), Insight into the nature of the ocean-continent transition off west Iberia from a deep multichannel seismic reflection profile, *Geology*, *24*, 1079–1082.

Reid, I. D. (1994), Crustal structure of a nonvolcanic rifted margin east of Newfoundland, *J. Geophys. Res.*, *99*, 15,161–15,180.

Sage, F., C. Basile, J. Mascle, B. Pontoise, and R. B. Whitmarsh (2000), Crustal structure of the continent-ocean transition off the Côte d'Ivoire-Ghana transform margin: Implications for thermal exchanges across the palaeotransform boundary, *Geophys. J. Int.*, *143*, 662–678.

Sahabi, M., D. Aslanian, and J. L. Olivet (2004), Un noveau point de départ pour l'histoire de l'Atlantique central (A new starting point for the history of the central Atlantic), *C. R. Geosci.*, *336*(12), 1041–1052, doi:10.1016/j.crte.2004.03.017.

Salisbury, M. H., and H. R. Jackson (2003), Crustal structure of the Meguma terrane parallel to the coast of Nova Scotia: Constraints on its origin, paper 42–1A presented at 38th Annual Meeting, Northeastern Sect., Geol. Soc. Am., Halifax, Nova Scotia.

Salisbury, M. H., and C. E. Keen (1993), Listric faults imaged in oceanic crust, *Geology*, *21*, 117–120.

Sandwell, D. T., and W. H. F. Smith (1997), Marine gravity anomaly from Geosat and ERS 1 satellite altimetry, *J. Geophys. Res.*, *102*, 10,039–10,054.

Sawyer, D. S., R. B. Whitmarsh, A. Klaus, and Shipboard Scientific Party (1994), *Proceedings of the Ocean Drilling Program, Initial Reports*, vol. 149, 719 pp., Ocean Drill. Program, College Station, Tex.

Sheridan, R. E., D. L. Musser, L. Glover III, M. Talwani, J. I. Ewing, W. S. Holbrook, G. M. Purdy, R. Hawman, and S. Smithson (1993), Deep seismic reflection data of EDGE U.S. Mid-Atlantic continental-margin experiment: Implications for Appalachian sutures and Mesozoic rifting and magmatic underplating, *Geology*, *21*, 563–567.

Shimeld, J. (2004), A comparison of salt tectonic subprovinces beneath the Scotian Slope and Laurentian Fan, in *Salt-Sediment Interactions and Hydrocarbon Prospectivity: Concepts, Applications, and Case Studies for the 21st Century, 24th Annual Bob. F. Perkins Research Conference* [CD-ROM], edited by P. Post, Gulf Coast Soc., Sect. of Econ. Paleontol. and Mineral., Houston, Tex., in press.

Srivastava, S. P., and C. E. Keen (1995), A deep seismic reflection profile across the extinct Mid-Labrador Sea spreading center, *Tectonics*, *14*, 372–389.

Talwani, M., J. L. Worzel, and M. Landisman (1959), Rapid gravity computations for two-dimensional bodies with application to the Mendocino submarine fracture zone, *J. Geophys. Res.*, *64*, 49–59.

Todd, B. J., I. Reid, and C. E. Keen (1988), Crustal structure across the southwest Newfoundland transform margin, *Can. J. Earth Sci.*, *25*, 744–759.

Wade, J. A., and B. C. MacLean (1990), The geology of the southeastern margin of Canada, in *The Geology of North America*, vol. I-1, *Geology of the continental margin of Eastern Canada*, *Geol. Can.*, no. 2, edited by M. J. Keen and G. J. Williams, pp. 167–238, Geol. Surv. of Can., Ottawa, Ont.

Welsink, H. J., J. D. Dwyer, and R. J. Knight (1989), Tectono-stratigraphy of the passive margin off Nova Scotia, in *Extensional Tectonics and Stratigraphy of the North Atlantic Margins*, edited by A. J. Tankard and H. R. Balkwill, *AAPG Mem.*, *46*, 215–231.

White, R. S., R. S. Detrick, M. C. Sinha, and M. H. Cormier (1984), Anomalous seismic crustal structure of oceanic fracture zones, *Geophys. J. R. Astron. Soc.*, *79*, 779–798.

White, R. S., D. McKenzie, and K. O'Nions (1992), Oceanic crustal thickness from seismic measurements and rare earth element inversions, *J. Geophys. Res.*, *97*, 19,683–19,715.

Whitmarsh, R. B., M.-O. Beslier, P. J. Wallace, and Shipboard Scientific Party (2000), *Proceedings of the Ocean Drilling Program, Initial Reports*, vol. 173, 493 pp., Ocean Drill. Program, College Station, Tex.

Williams, H. (1979), Appalachian Orogen in Canada, *Can. J. Earth Sci.*, *16*, 792–807.

Williams, H. (1995), Temporal and spatial divisions, in *Geology of the Appalachian-Caledonian Orogen in Canada and Greenland*, *Geol. Can.*, no. 6, edited by H. Williams, pp. 21–44, Geol. Surv. of Can., Ottawa, Ont.

Zelt, C. A., and D. A. Forsyth (1994), Modeling wide-angle seismic data for crustal structure: Southeastern Grenville Province, *J. Geophys. Res.*, *99*, 11,687–11,704.

Zelt, C. A., and R. B. Smith (1992), Seismic traveltime inversion for 2–D crustal velocity structure, *Geophys. J. Int.*, *108*, 16–34.

S. A. Dehler and H. R. Jackson, Geological Survey of Canada (Atlantic), Bedford Institute of Oceanography, P.O. Box 1006, Dartmouth, Nova Scotia, Canada B2Y 4A2. (sdehler@nrcan.gc.ca; rujackso@nrcan.gc.ca)

T. Funck, Danish Lithosphere Centre, Øster Voldgade 10, L, 1350 Copenhagen K, Denmark. (tf@dlc.ku.dk)

K. E. Louden, Department of Oceanography, Dalhousie University, Halifax, Nova Scotia, Canada B3H 4J1. (Keith.Louden@dal.ca)

Y. Wu, Department of Earth Sciences, Dalhousie University, Halifax, Nova Scotia, Canada B3H 3J5. (wuyue@phys.ocean.dal.ca)